A novel method for analogue modelling of lithospheric-scale rifting, monitored through X-Ray CT-scanning, at the University of Bern Tectonic Modelling Laboratory (Switzerland) (https://doi.org/10.5880/fidgeo.2023.005)

Frank Zwaan[1,2] & Guido Schreurs[1]

1. *University of Bern, Institute of Geological Sciences, Baltzerstrasse 1+3, 3012 Bern, Switzerland*
2. *Helmholtz Centre Potsdam - GFZ German Research Centre for Geosciences, Telegrafenberg, 14473 Potsdam, Germany*

1. Licence

2. Citation

When using the data please cite:

Zwaan, F., & Schreurs, G. (2023) A novel method for analogue modelling of lithospheric-scale rifting, monitored through X-Ray CT-scanning, at the University of Bern Tectonic Modelling Laboratory (Switzerland). GFZ Data Services, https://doi.org/10.5880/fidgeo.2023.005

The data are supplementary material to:

Zwaan, F., & Schreurs, G. (2023). Analogue models of lithospheric-scale rifting monitored in an X-ray CT scanner. Tectonics, 42, e2022TC007291. https://doi.org/10.1029/2022TC007291

3. Table of contents

1. Licence 1
2. Citation 1
3. Table of contents 1
4. Data Description 2
   4.1. Background 2
   4.2. Concept and model design 3
   4.3. Model monitoring and analysis 9
      4.3.1. Time-lapse photography analysis 9
      4.3.2. CT-scanning 12
   4.4. Modelling protocol used by Zwaan & Schreurs (2023a). 15
   4.5. Challenges 23
      4.5.1. Mechanical leeway 23
      4.5.2. Visualization of model layering on CT-imagery - testing 23
   4.6. Potential for future modelling studies 29
5. Acknowledgements 30
6. References 30

4. Data Description

This data set is a description of a novel analogue modelling method used to run lithospheric-scale tectonic models, and to uniquely monitor these models through X-Ray CT-scanning techniques at the Tectonic Modelling Lab of the University of Bern (Switzerland). It includes information on the model set-up and model materials, and includes a step-by-step description of the general modelling procedure. A first application of this novel procedure, for the simulation of lithospheric scale rifting processes can be found in Zwaan & Schreurs (2023a) in Tectonics, with supplementary data publication via GFZ Data Services (Zwaan & Schreurs 2023b). The results of this work prove the feasibility of the method, and opens the door to a broad variety of new tectonic modelling studies.

4.1. Background

To study lithosphere-scale rifting, analogue tectonic modellers have routinely applied set-ups involving a model lithosphere floating on top of a heavy fluid (e.g. syrup or honey) that represents the asthenosphere, allowing for isostatic compensation (e.g. Allemand & Brun 1991; Benes & Davy 1996; Benes & Scott 1996; Brun & Beslier 1996; Sun et al. 2009; Capelletti et al. 2013; Autin et al. 2010, 2013; Nestola et al. 2013, 2015; Molnar et al. 2017, 2018; Beniest et al. 2018; Samsu et al. 2021, Fig. 1). Deformation is generally induced by moving a U-shaped sidewall situated in a basin containing the heavy fluid outward, pulling the model lithosphere apart, with the edges of this U-shaped sidewall acting as velocity discontinuities that focus deformation, inducing asymmetric rifting (Fig. 1a).

On-going advances in model monitoring techniques have allowed researchers to analyse model surface deformation in great detail. However, an important issue with this type of experiments is that the internal deformation of the model lithosphere cannot be directly observed. Only after completing the model run, layers can be removed to reveal internal structures (Nestola et al. 2015), or cross-sections can be made (e.g. Allemand et al. 1989; Brun & Beslier 1996).

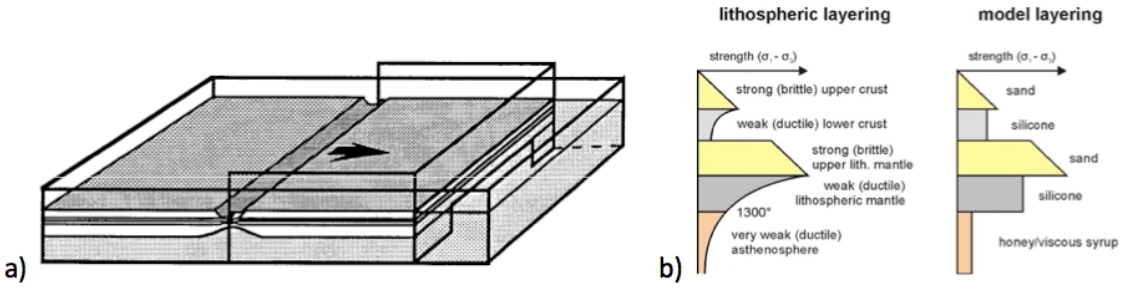

Figure 1. (a) Example of lithospheric-scale rifting model set-up. (b) Natural strength profile of a typical 4-layer lithosphere and the types of materials used to reproduce this strength profile in analogue models. Based on Beslier (1991).

This monitoring issue can be solved by applying CT-scanning techniques (e.g. Richard 1989; Colletta et al. 1991; Sassi et al. 1993; Letouzey et al. 1995), which have been a specialty of the Tectonic Modelling Laboratory in Bern (e.g. Schreurs et al. 2002a, 2002b, 2003, 2006, 2016; Panien et al. 2005, 2006, Adam et al. 2013; Alonso-Henar et al. 2015; Zwaan & Schreurs 2015, 2017, Zwaan et al. 2016, 2018a, 2019, 2020b, 2021a; Zwaan 2017; Fedorik et al. 2019; Schori et al. 2021; Schmid et al. 2022a, 2022b). The CT-scanning solution in Bern is made possible by a close partnership with the Institute of Forensic Medicine (IRM) at the University of Bern,

especially with the help from Nicole Schwendener, but was until now never applied to lithospheric-scale analogue models of rifting.

4.2. Concept and model design

The first inspiration to run lithospheric-scale models of rifting in a CT-scanner was developed through discussions with Yago Nestola, who was working at the University of Parma at the time, and who had experience with modelling lithospheric-scale rifting (Nestola et al. 2013, 2015). The initial idea was to reproduce his previous models by building a similar set-up to be put onto the already existing Namazu machine in Bern (which was designed as part of the PhD project by Matthias Klinkmüller [Klinkmüller 2011, Fig. 2], based on another machine at IFP Energies Nouvelles in Rueil Malmaison, Paris (e.g. Schreurs & Colletta 1998, 2002). Unfortunately, this idea did not come into practice due to a lack of time and resources.

Subsequently, the original idea evolved into a more ambitious concept (Zwaan 2017), which aimed to make use of the versatility of the Namazu machine (Fig. 3), in order to include options for oblique movements as well. This new concepts was refined and realized, as part of a Swiss National Science Foundation-funded project 200021-178731 (http://p3.snf.ch/Project-178731) (Fig. 4). The refining and realization of the concept was done by engineers from IPEK Rapperswil (Dario Niggli, Peter Eichenberger and Theodor Wüst), as part of a long-standing partnership between the lab in Bern and IPEK; students and employees from IPEK (Reto Gwerder, Rudolf Kamber, Michael Ziltener, Christoph Zolliker, Claude Grau, Theodor Wüst and Yves Pöltinger) have supported the lab in Bern in various ways, i.e. by building the Namazu machine (Klinkmüller 2011), designing and improving new parts for that machine (e.g. Zwaan et al. 2016; Zwaan 2017), as well as upgrading its operating software, and designing and constructing a new machine allowing for the simulation of rotational tectonics (Zwaan 2017; Zwaan et al. 2020b; Schmid et al., 2022a, b).

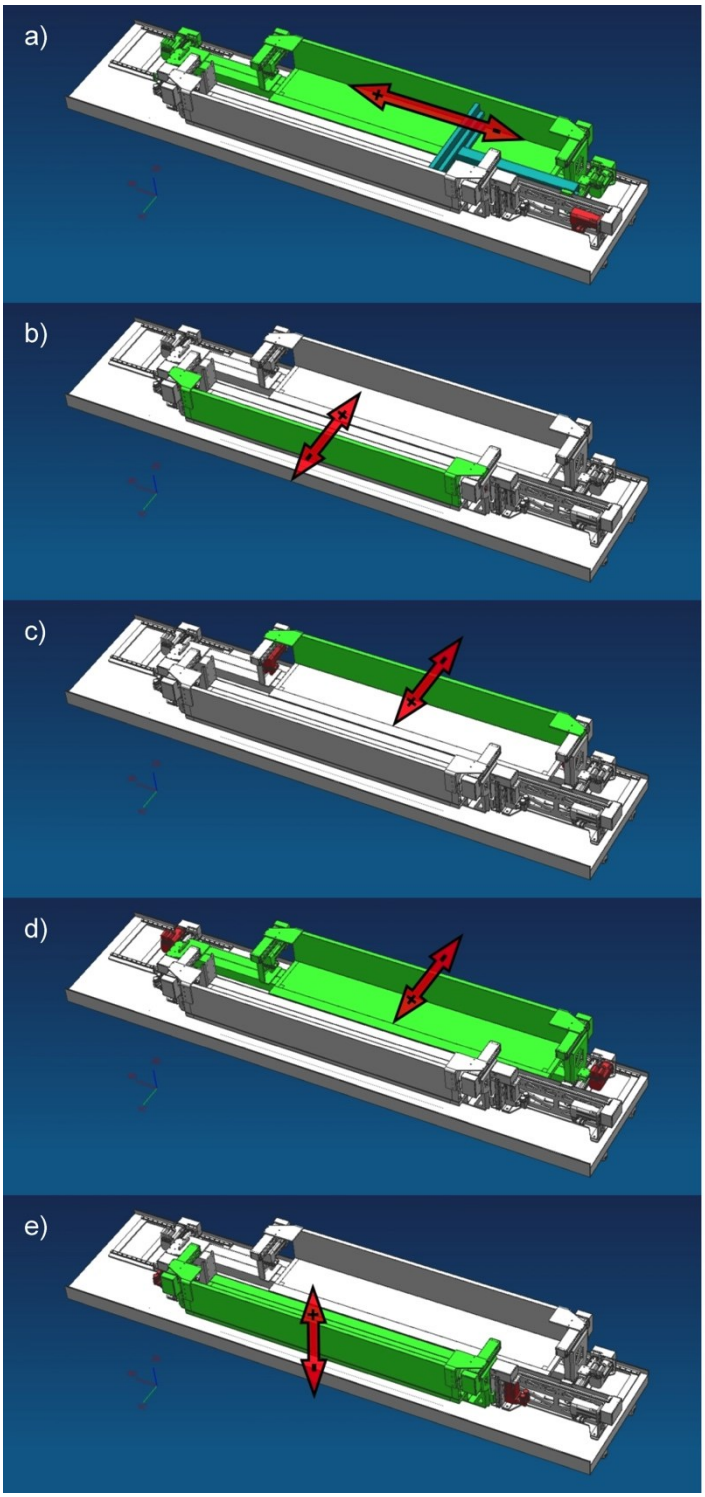

X1-axis, controls lateral or strike-slip motion. Positive motion is left-lateral, negative motion is right-lateral. The special blue part indicated in the figure can be attached to the X1 axis for along-strike compression models.

Y1-axis, controls motion of the Y1 longitudinal sidewall. Positive motion is compressional, negative motion is extensional.

Y2-axis, controls motion of the Y2 longitudinal sidewall. Positive motion is compressional, negative motion is extensional.

Y3-axis, controls motion of the X1 base plate. When this axis moves, the Y2 sidewall moves with it, as it is mounted on top of the base plate. Positive motion is compressional, negative motion is extensional.

Z1-axis, controls vertical motion of the X2 base plate. When this axis moves, the Y1 sidewall moves with it, as it is mounted on top of the base plate. Positive motion is up-ward, negative motion is downward.

Figure 2. Overview of the various components of the Namazu experimental apparatus and their respective motion directions controlled by axes (Y1-3, X1 and Z1). After Zwaan (2017).

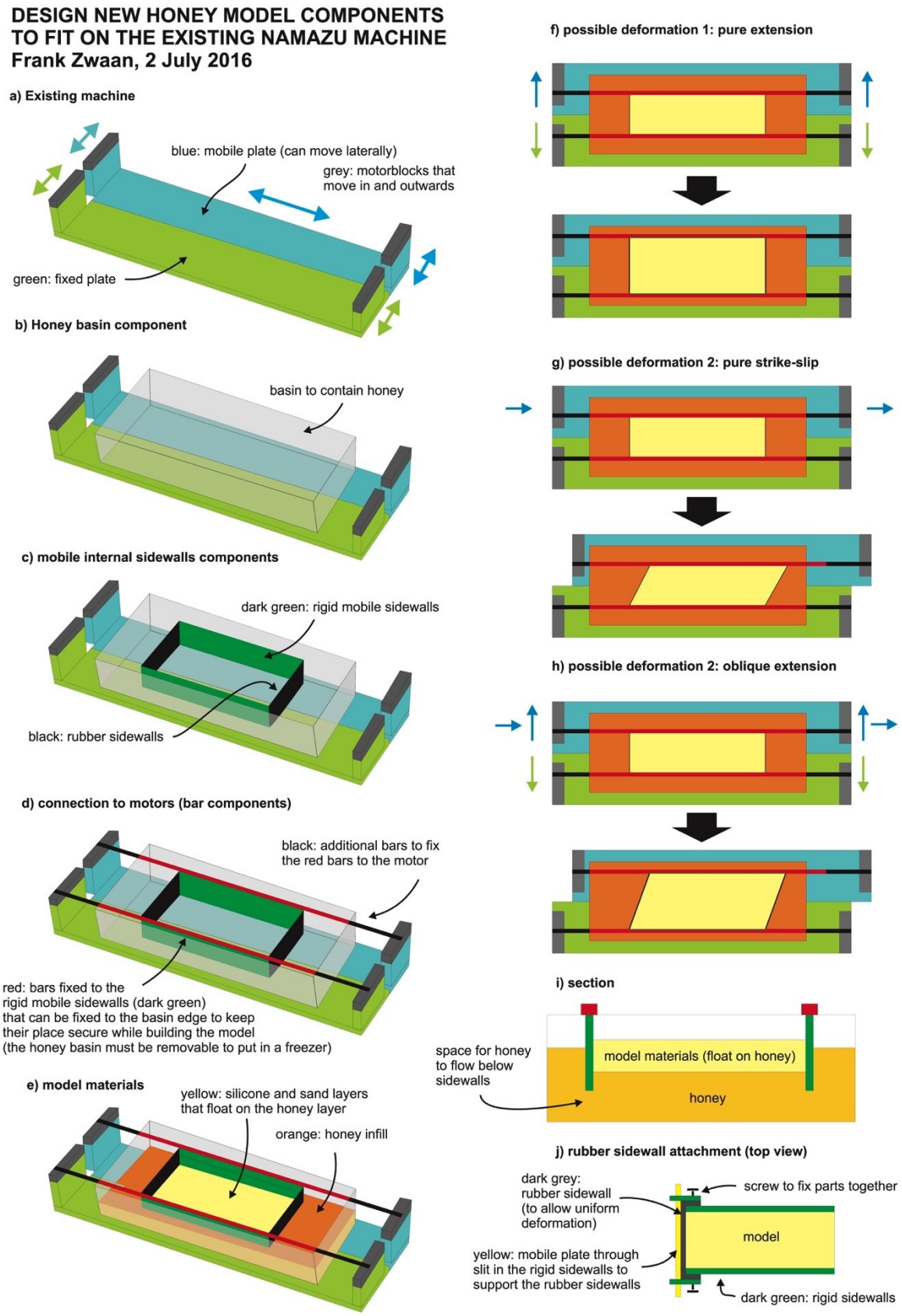

Figure 3. Initial design of the new set-up for lithospheric-scale rift models (after Zwaan, 2017).

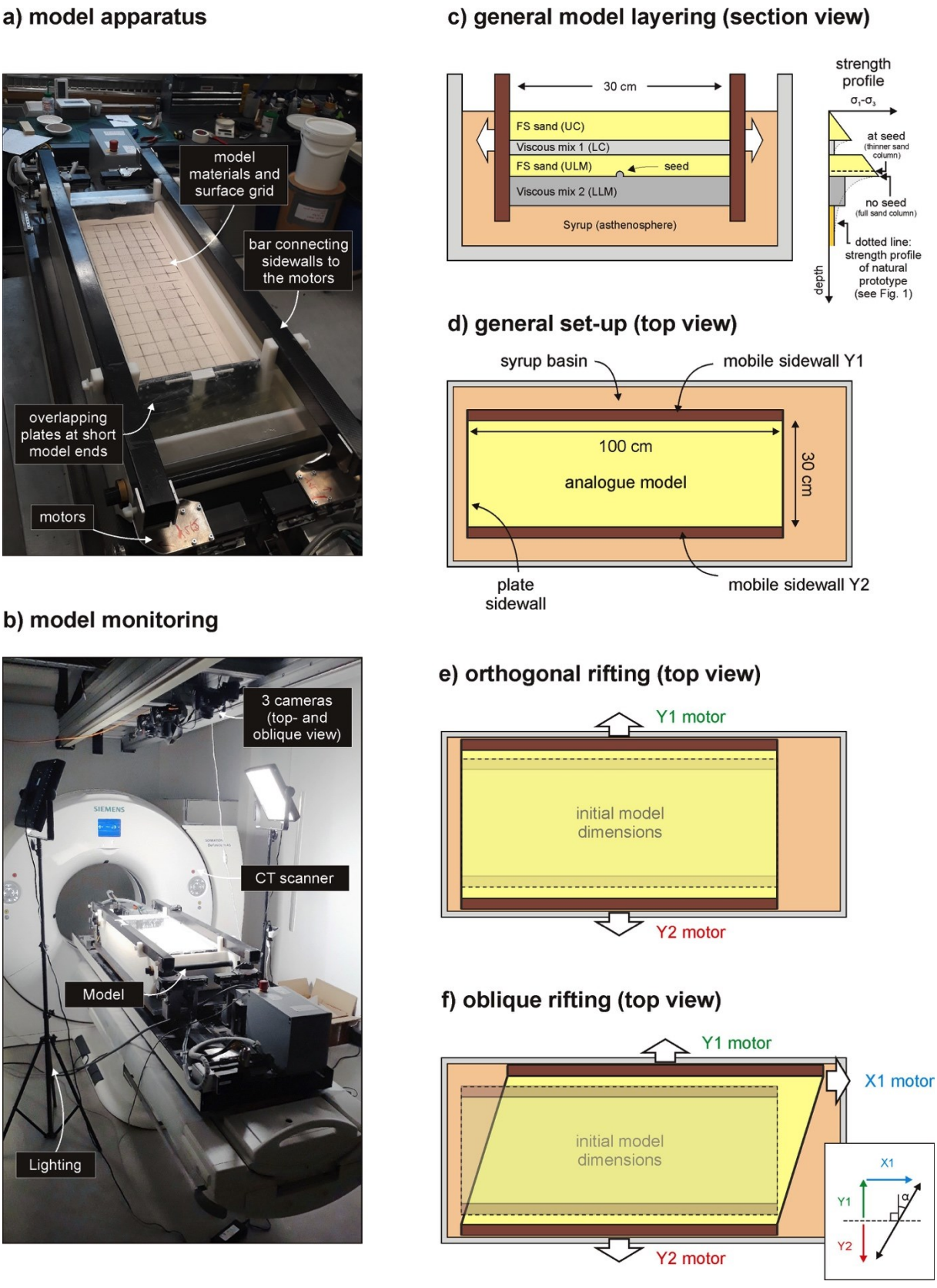

Figure 4. Final design of the new method for modelling lithospheric-scale rifting (after Zwaan & Schreurs, 2023a).

The basic design of our new lithospheric-scale set-up is in principle quite similar to previous work (e.g. Allemand et al. 1989; Nestola et al. 2013, 2015, Fig. 1); it involves a (multilayer)

lithosphere (consisting of brittle and viscous layers) put in a basin containing a high-density low-viscosity liquid (glucose syrup) that represents the asthenosphere, on which the model lithosphere floats. The system is however different in that we have two longitudinal inner sidewalls hanging into the syrup that contain the model lithosphere floating on top of the syrup, instead of a single U-shaped sidewall (Figs. 1, 4). We can also induce orthogonal (symmetric) rifting in our set-up by simply moving the inner sidewalls, which are linked to the computer-controlled Y1 and Y2 motors of the Namazu machine, apart (Figs. 2-4).

A further important difference to most other model set-ups for lithospheric-scale rifting is the ability to apply oblique extension. This is achieved through the addition of lateral motion of the X-1 motor (Figs. 3g, h, 4f), so that we can combine strike-slip deformation with orthogonal extension to obtain different degrees of oblique extension (or compression). Importantly, these different styles of deformation (orthogonal and oblique rifting) are accommodated by the short sidewalls, of which we have two types: overlapping plates (rather similar to the U-forms in standard models), or rubber sidewall (creating distributed deformation along the sidewalls, as used in previous analogue models of crustal-scale rifting in Bern, e.g. Zwaan et al. 2016, 2018a, 2019, 2020b).

Other practicalities involve the choice of material used to build the set-up, as well as the model itself, since all materials need to be made out of X-ray transparent materials. The set-up itself is made out of plastic and carbon fibre. To model the asthenosphere, we use Glucosweet 44 glucose syrup manufactured by A.D.E.A. S.rl. (https://www.adea-srl.it/), of which the rheological properties were determined in collaboration with colleagues from the University of Roma TRE (Schmid et al. 2022c). The syrup has a density of ca. 1450 kg/m^3, and since the model lithosphere must float on it, the standard materials used in Bern (quartz sand or corundum sand from Carlo Bernasconi AG [https://www.carloag.ch], to simulate brittle layers, and a ca. 1:1 weight ratio viscous mixture made of SGM-36 PDMS (silicone) and corundum sand to simulate ductile layers in nature, both with densities > 1500 kg/m^3, (e.g. Zwaan et al. 2016, and Table 1 in Section 4.5.2 of this data publication) are not appropriate. Instead we use the FS900F feldspar sand provided by Quartzwerke Gruppe (or Amberger Kaolinwerke, https://www.quarzwerke.com) as our brittle analogue material; this feldspar sand has a relatively low density of ca. 1300 kg/m^3 when sieved, and appropriate internal friction angles for simulating brittle materials in the lithosphere (Willingshofer et al. 2018; Zwaan et al. 2022b). Furthermore, we apply mixtures of polydimethylsiloxane (PDMS) and corundum sand with a lower corundum sand content to obtain viscous materials with densities <1450 kg/m^3 (and known rheology, Zwaan et al. 2018c), so that they may float on the syrup. We furthermore tested Liaver and Zirshot foam beads to add internal layering that is visible on CT-imagery (more details in section 4.5).

In order to prepare a model run, we first need to stabilize (freeze) the syrup since there is no place for compensation of vertical motion by vertically mobile sidewalls as for instance used by Molnar et al. (2017) (Fig. 5b). The whole model must after all fit in the CT-scanner (Fig. 3b), and the relatively large size of model compared to the relatively small size of the syrup basin means that vertical motion of the model cannot be easily compensated. If this is not done correctly, the model may simply sink to the base of the syrup basin, while parts of the model will remain sticking to the sidewalls, creating an overall sag effect (Fig. 5a). To make sure the syrup is stable during model preparation, we need a deep-freezer (both capable of containing

the basin and freezing the syrup to -30˚C in order to make it sufficiently rigid, if not solid, Fig. 6). After inserting the model layers, it is of great importance to add the correct volume of syrup to the basin in order to counteract the sinking of the modelled lithosphere into the syrup after the latter thaws (Fig. 5c).

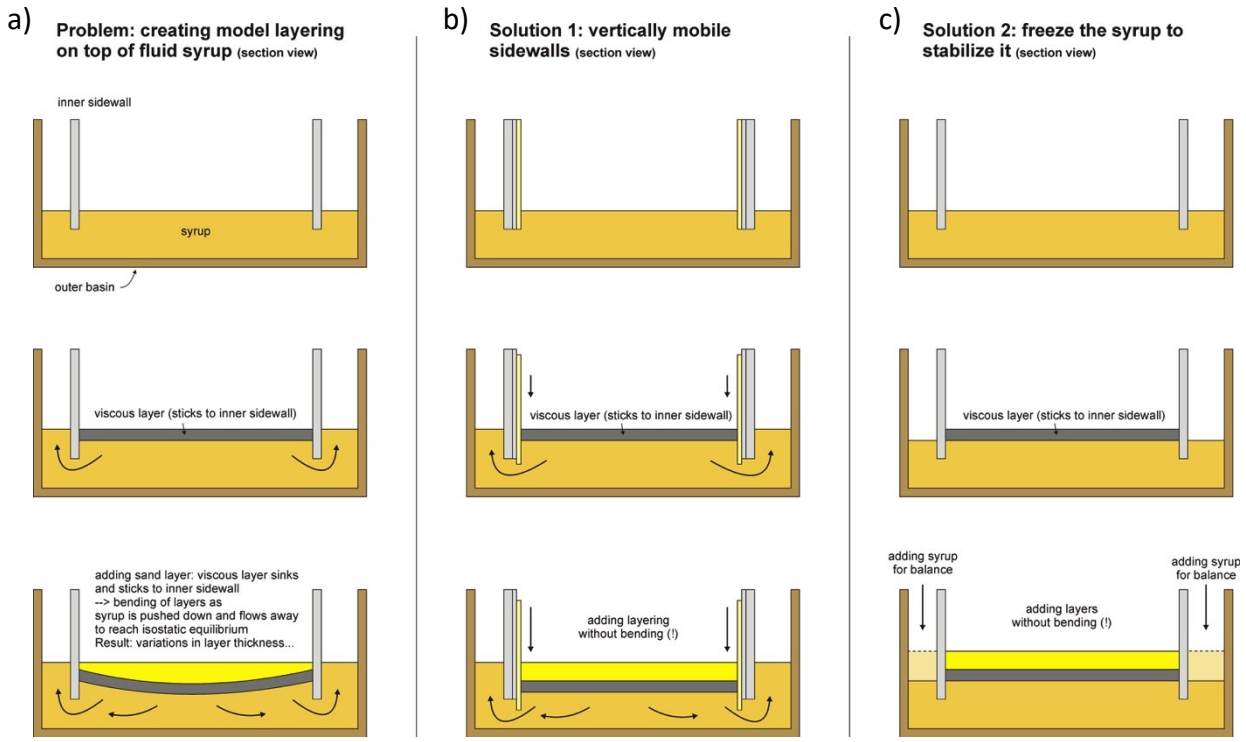

Figure 5. Explanation of the need for stabilizing the syrup and either adding syrup, or a mechanism to allow for vertical motion to compensate for added weight (i.e. the model layers). (a) Undesirable deformation during model preparation as the syrup flows away below the model layers. (b) First solution: vertically mobile inner sidewalls, allow layers to sink without bending as syrup flows away. (c) Second solution, used in our (Zwaan & Schreurs 2023a) models: freeze the syrup before adding the layers, and add extra syrup to compensate for syrup flow that would otherwise occur after thawing of the syrup.

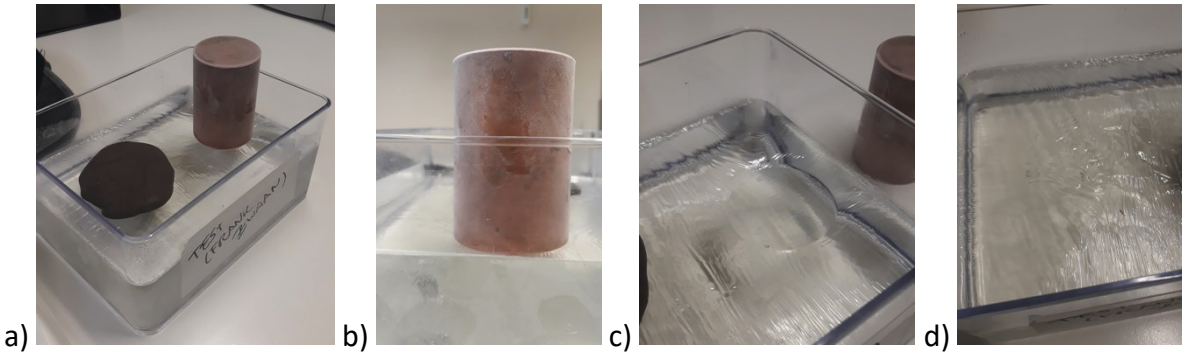

Figure 6. Stability test of frozen glucose syrup (-30˚C). The metal weight caused a moderate footprint on the syrup surface. The patch of viscous material had no clear impact. Box length: ca. 20 cm. Wrinkles on the syrup surface disappear after thawing, and in models these wrinkles are compensated and flattened by flow of the overlying viscous layer.

4.3. Model monitoring and analysis

We use various techniques to monitor and analyse our models and the deformation, including model surface time-lapse analysis, topography analysis, CT-scanning, and digital image correlation (DIC) analysis on both time-lapse model surface imagery and CT-data. Various combinations have been regularly used in our lab over the course of the last years (e.g. Alonso-Henar et al. 2015; Zwaan et al. 2016, 2018a, 2020b, 2021a, 2022a; Zwaan & Schreurs 2017, 2020, 2023a; Fedorik et al. 2019; Schori et al. 2021, Schmid et al. 2022a, 2022b).

4.3.1. Time-lapse photography analysis

We use a rig containing three high-resolution D810 Nikon cameras, one of which provides top view images, and the other two inclined (stereoscopic) images of the model surface (Fig 4b). These cameras are programmed via a computer to create time-lapse series (for more details on the camera set-up, time-lapse software and hardware, see Schmid et al. (2022a, 2022b). At the same time, we use a timer for the lighting on one side of the model to switch on and off, so that we obtain a time series of images with, and without shading (Fig. 7).

The images with shading are made to obtain direct visual observations regarding surface deformation (the shading highlighting surface structures), whereas the images without shade are ideal for automated 2D (map view) strain analysis. The strain analysis is done using DaVis DIC software from LaVision (www.lavision.de), which compares surface patterns on images (if needed after correction for their inclination using pictures of a calibration plate with know dimensions) from different time steps and detects deformation. The result is a detailed and quantified analysis of surface model deformation over time (Fig. 8f-j). For more details on this analysis method, see e.g. Boutelier et al. (2019) and Schmid et al. (2022a, 2022b).

Furthermore, the inclined images, preferably without shade, allow for stereoscopic reconstruction of the model topography over time through photogrammetry software such as Agisoft Photoscan (www.agisoft.com). By comparing the different distortions of the images from the stereoscopic images, such software can reconstruct the 3D model surface for selected time steps. It may be noted that DaVis can also be used for topography analysis (Schmid et al. 2022a, 2022b). These 3D surfaces should be georeferenced using reference markers with known coordinates placed (in view) on the model set-up (or in the case of 3D DIC by a calibration plate), to produce properly georeferenced digital elevation models (DEMs). These DEMs can subsequently be post-processed in geographic information system (GIS) software, such as QGIS (www.qgis.org) (Fig. 8a-e).

a) t = 0 min (shade)

d) t = 0 min (no shade)

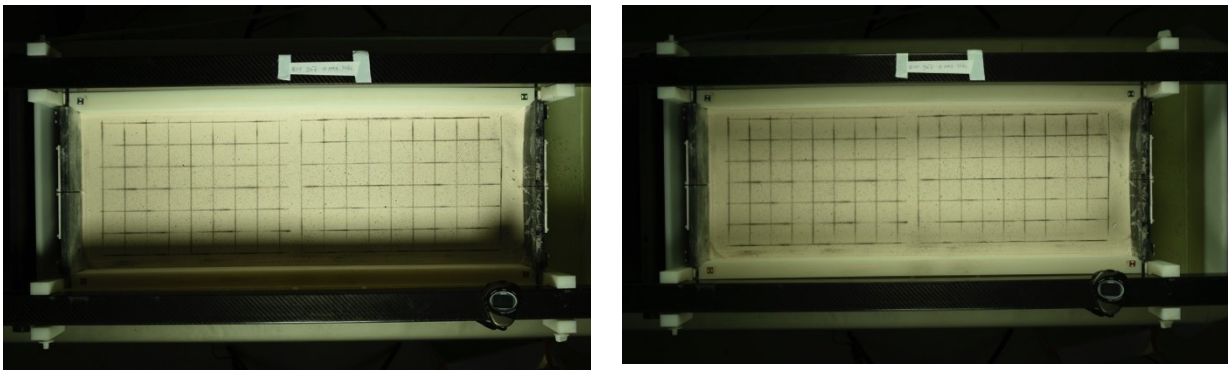

b) t = 120 min

e) t = 120 min (no shade)

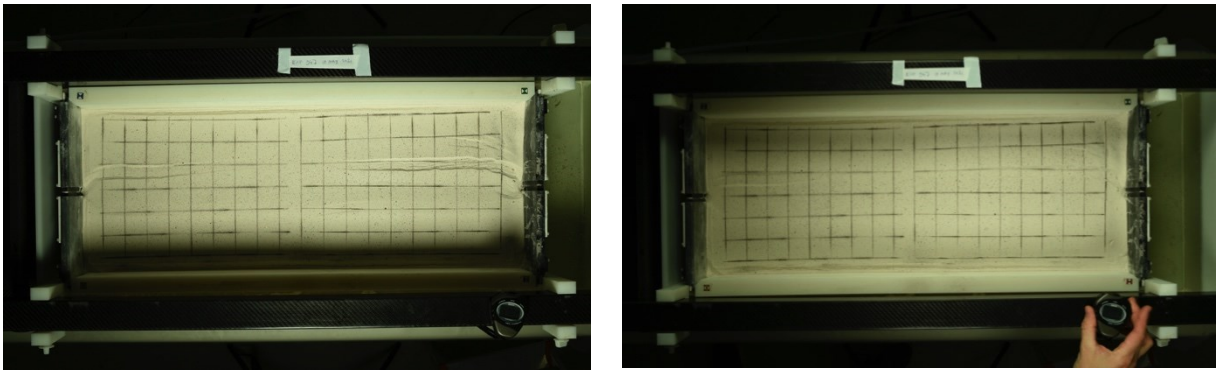

c) t = 300 min

f) t = 300 min (no shade)

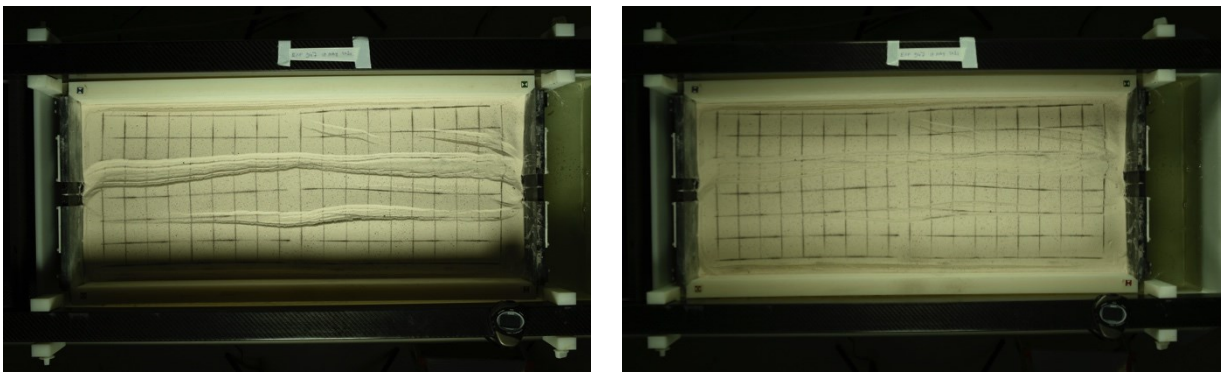

Figure 7. Time-lapse imagery of Model C from Zwaan & Schreurs (2023a). (a-c) with shading (to highlight surface structures), and (d-f) without shading (for DIC analysis)

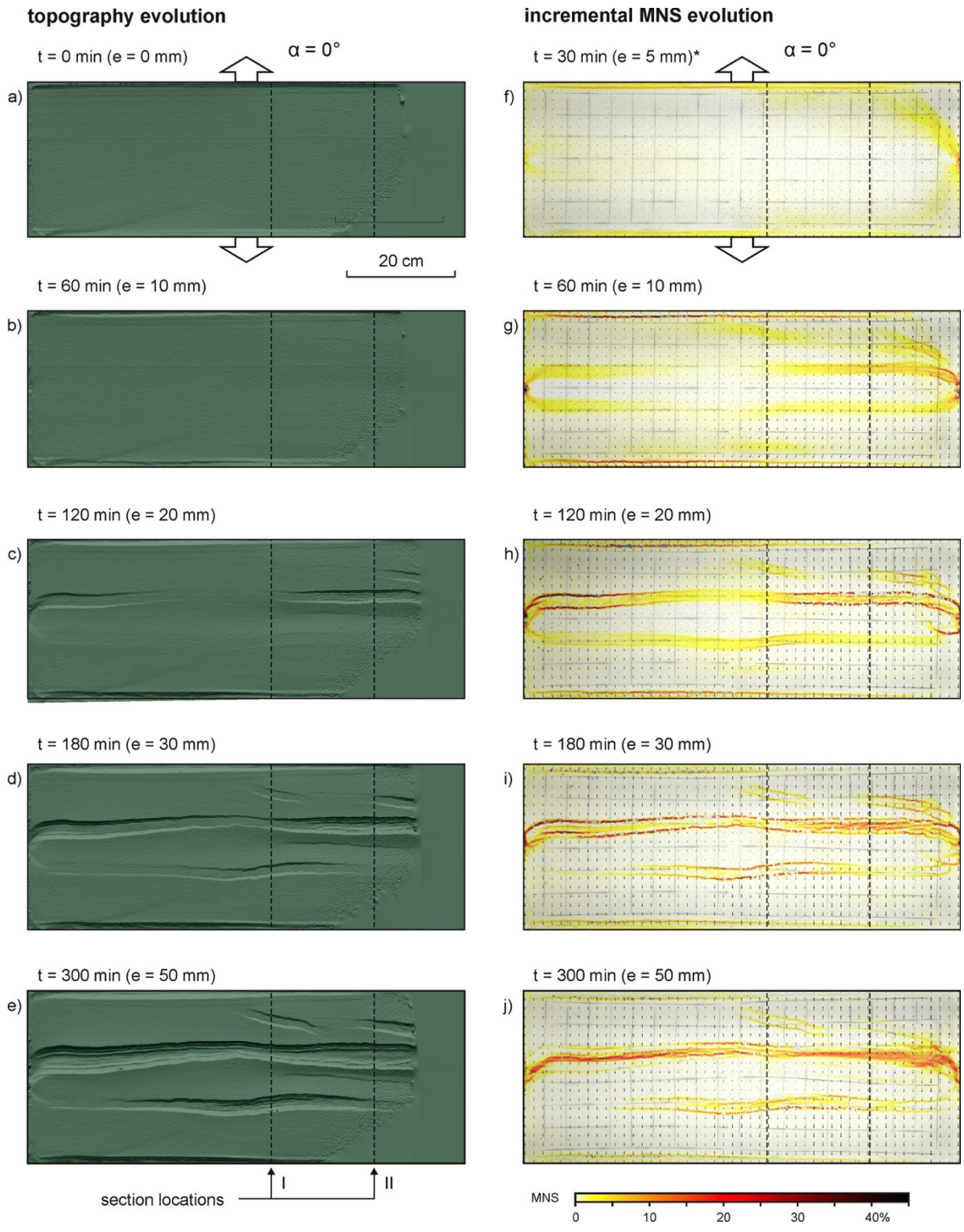

Figure 8. Topography and DIC analysis overview of Model C from Zwaan & Schreurs (2023a) (a-e) Topography analysis results, lighting from top. (f-j) DIC (incremental MNS [maximum normal strain]) analysis, representing the length of the longest axis of the strain ellipse in the horizontal plane, which is taken as a proxy for normal fault development.

4.3.2. CT-scanning

Next to 3D time-lapse photography and the quantitative surface analyses it enables, X-Ray CT-scanning allows us to for the first time trace the internal 3D structural evolution of this type of models (Fig. 9, 10). Until now, CT-scanning (including the work by Schmid et al. 2022a, 2022b, and Zwaan & Schreurs 2023a) was done using the 64 slice Siemens Somatom Definition AS apparatus at the Institute of Forensic Medicine of the University of Bern. The CT-scanner has recently been replaced with a 64-slice Siemens Somatom X.cite with a larger (82 cm) gantry bore diameter. For practical reasons, the central 50 cm of each analogue model completed by Zwaan & Schreurs (2023a) was selected for CT-scanning, but the size of the scanning volume (along with various other scanning parameters) can be modified if required. CT data can be subsequently visually analyzed in DICOM viewers, e.g. Horos (https://horosproject.org/). Such software creates 3D cubes out of the individual CT-scans (i.e. serial sections taken perpendicular to the model axis), and allows detailed inspection and sectioning in all directions and over time (Figs. 9, 10), very similar to the visualization of 3D seismic datasets in e.g. Petrel. Furthermore, CT sections can also be used for 2D DIC analysis in DaVis, providing the first-ever quantified insights of internal deformation of analogue models of lithospheric-scale rifting (Fig. 11).

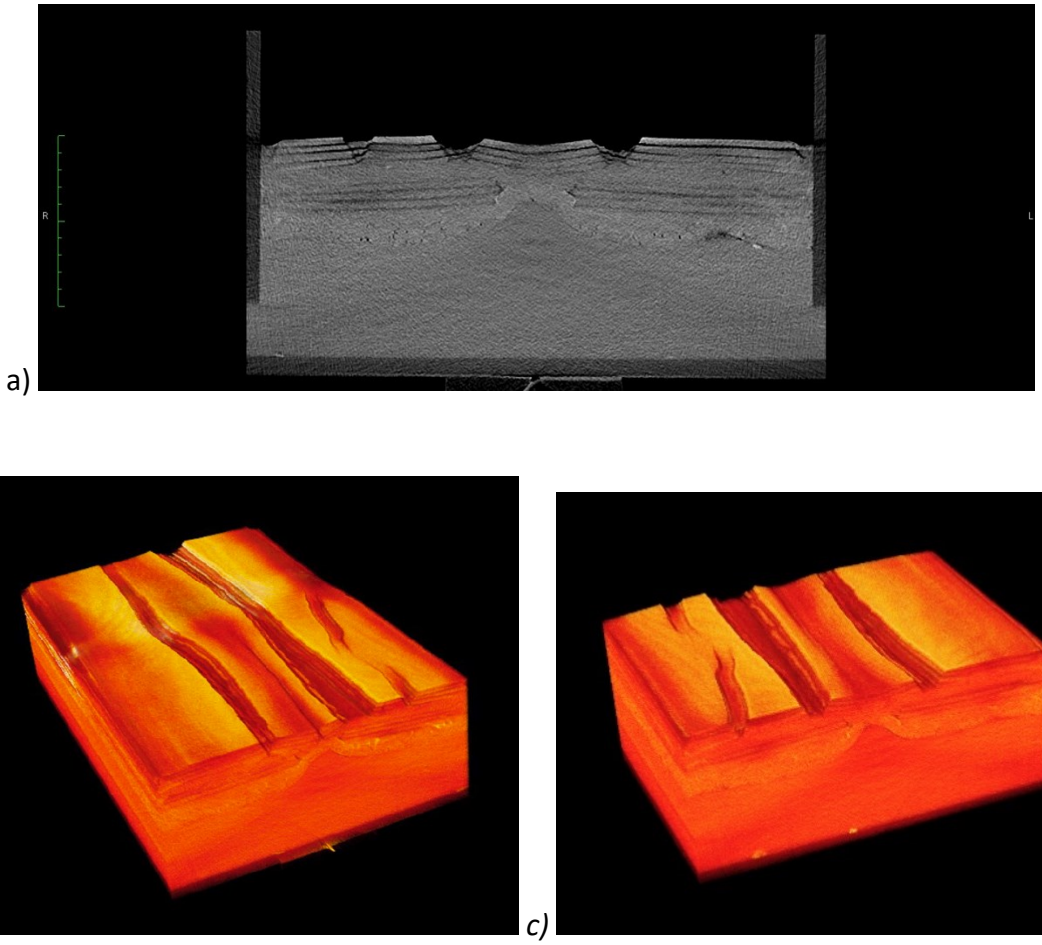

Figure 9. CT data depicting the final state of model C from Zwaan & Schreurs (2023a). (a) CT cross-section. (b-c) Different renderings of 3D CT imagery. Model width: ca. 30 cm.

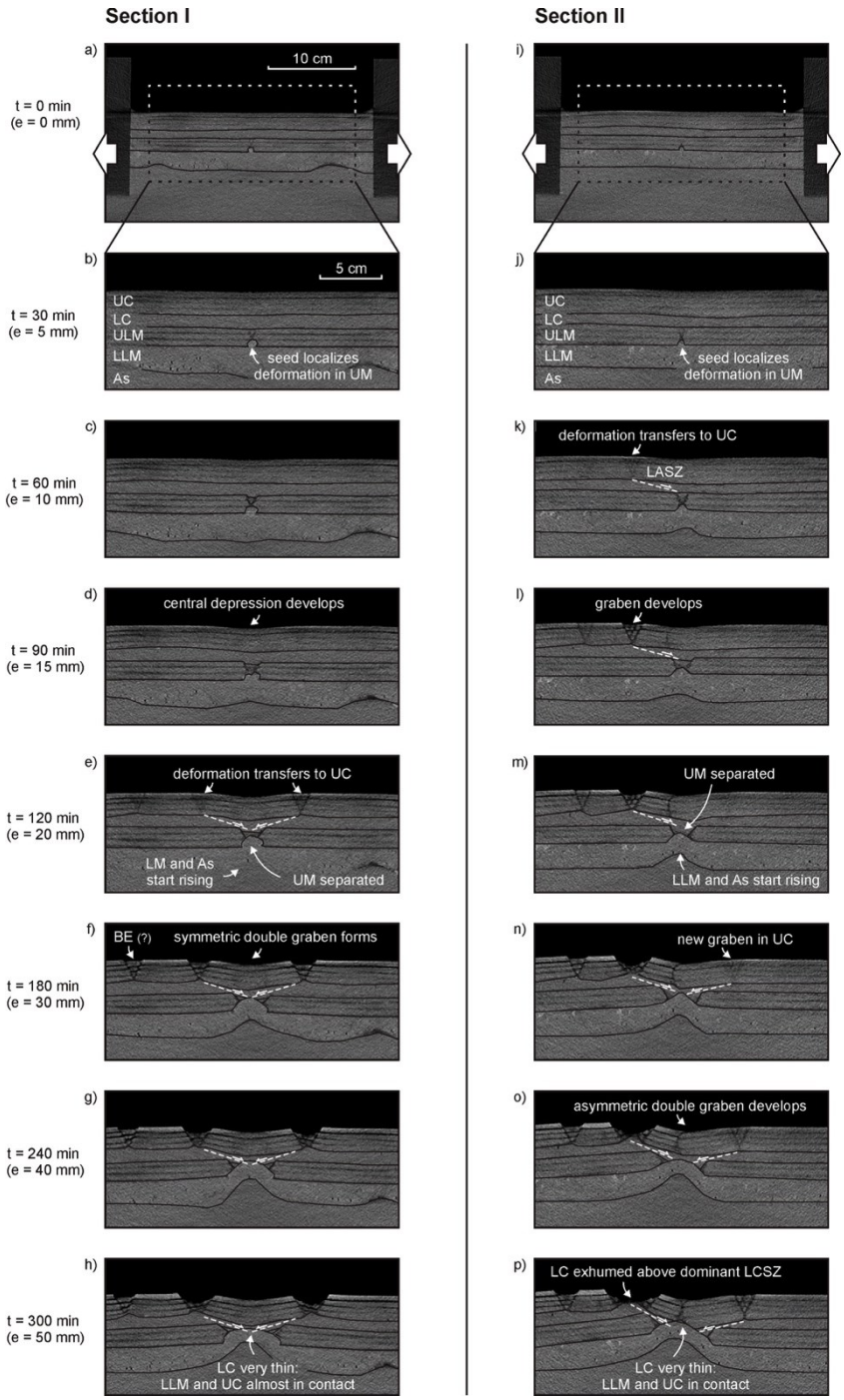

Figure 10. CT sections I and II depicting the internal evolution of the symmetric and asymmetric double rift systems found in Model C from Zwaan & Schreurs (2023a). Dark lines are added to highlight layer contacts. LC: lower crust, LLC: lower lithospheric mantle. As: asthenosphere, LASZ: low-angle shear zone, LC: lower crust, LLM: lower lithospheric mantle, ULM: upper lithospheric mantle, UC: upper crust. CT section locations are indicated in Fig. 8.

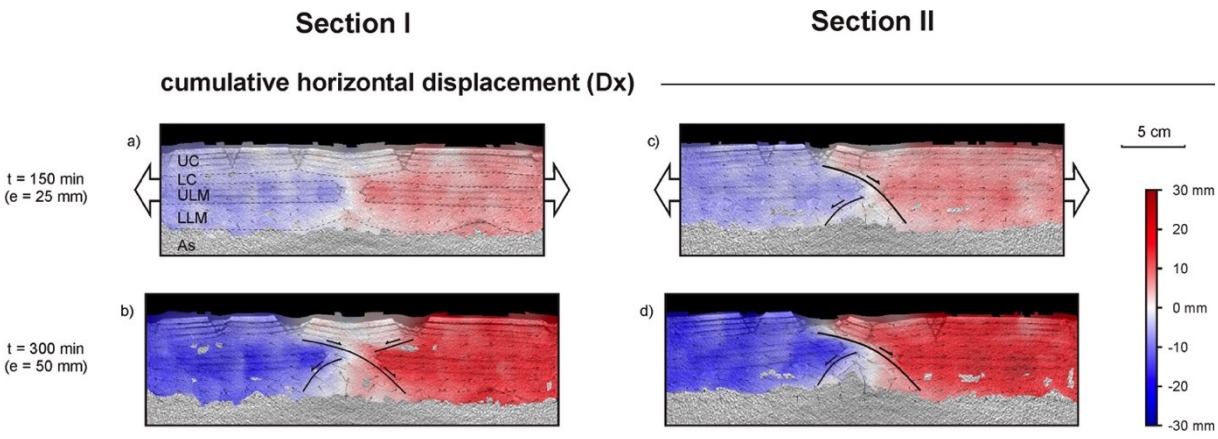

Figure 11. Results of DIC analysis on CT sections I and II from Model C from Zwaan & Schreurs (2023a). Cumulative horizontal displacement (Dx) as seen in section. Section locations indicated in Fig. 8.

4.4. Modelling protocol used by Zwaan & Schreurs (2023a).

Below we describe the general protocol used by Zwaan & Schreurs (2023a) for preparing and running lithosphere-scale analogue models that were monitored in a CT-scanner. The abbreviations used in the text are the following: LC: viscous lower crust, LLM: viscous lower lithospheric mantle, UC: brittle upper crust, ULM: brittle upper lithospheric mantle.

Step 1. Prepare materials (mixture[s]) about a week in advance so that air bubbles in the mixture have time to escape. The mixture(s) should have lower densities than the basal syrup layer to float. Make sure to have sufficient granular materials of an appropriate low density when sieved (e.g. Feldspar sand).

Step 2. Fill frames (with plastic sheet base) with appropriate amounts of viscous mixtures (i.e. silicone [PDMS] mixed with corundum sand) simulating the LC and LLM, and let them flow out on a flat surface (make sure it is level). The best way to make such frames is by compiling them from separate pieces of plexiglass taped together, put on top of a plastic sheet (Fig. 12). Use weights to make sure that the frame is fixed, so that no viscous material can flow below it.

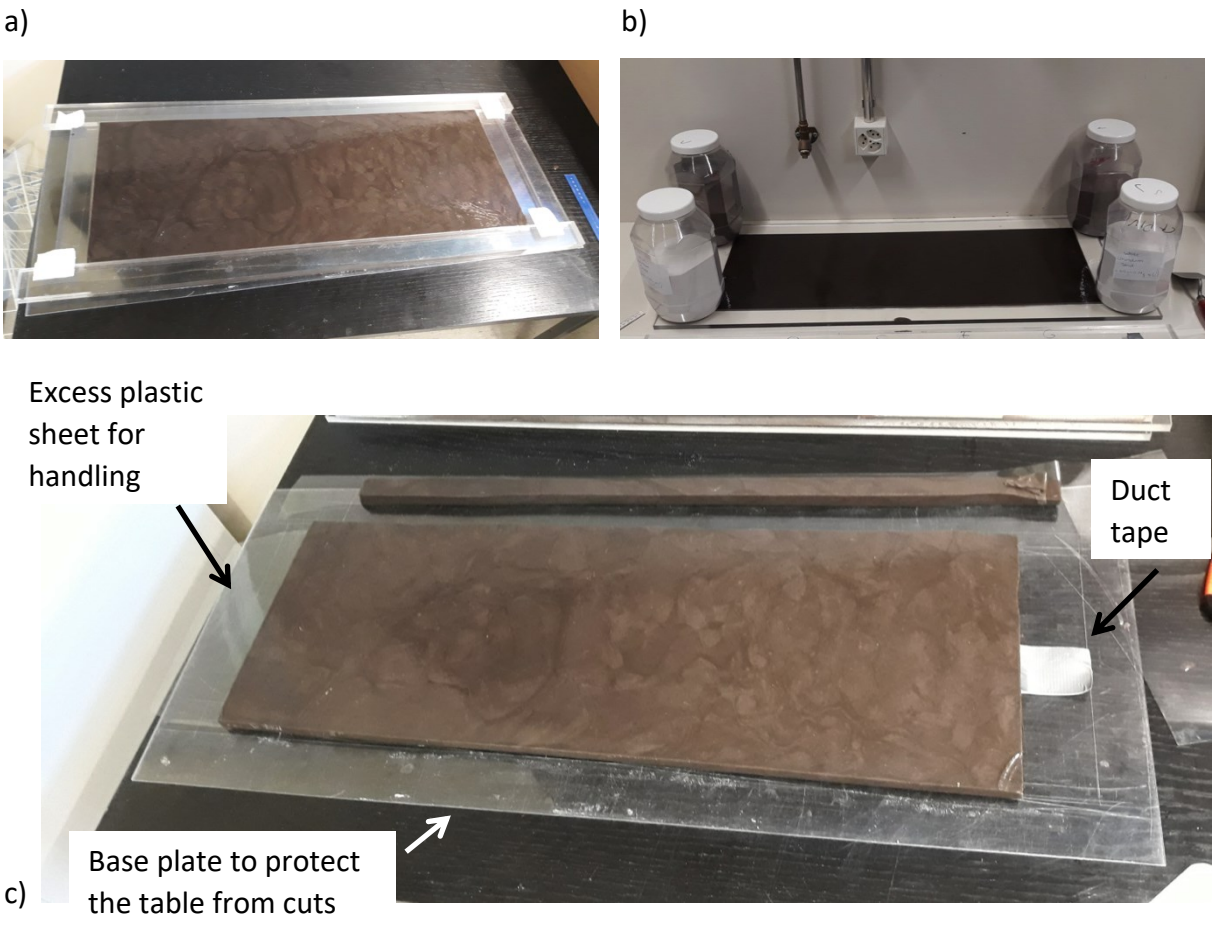

Figure 12. Example of frame used for preparing viscous layering. (a) Preparing the frame, out of plastic parts (b) securing the frame so that no material can flow below it. (c) Cutting the viscous layer away the frame. Note that to the left, an excess piece of the basal plastic sheet is still present for handling purposes. For handling and adding the viscous layer to the model, also some duct tape is added to the basal sheet, visible to the right.

Step 3. Fill the outer basin with glucose syrup and let it flow out to the appropriate level. As the syrup is very sticky, use tools used for cooking and handling liquids (e.g. spatulas, measuring cups), and avoid direct contact with the syrup to avoid creating a sticky mess.

Step 4. Add the inner sidewalls parts (choose between the plate or rubber short sidewall options) and let the syrup accommodate (only if these sidewalls were not left in the syrup from a previous model run) (Fig. 13).

Step 5. Fix the inner sidewalls to the outer basin (with four plastic screws in each corner, Fig. 13)

Figure 13. Syrup in the basin, with the inner sidewalls hanging in it. Note the dark material, which is leftover viscous material from a previous model. The inner sidewalls are fixed in place (i.e. by screws to the syrup basin), and the syrup is frozen, causing a subtle wrinkling on its surface.

Step 6. Cover the basin with the custom-made lid that fits around the inner sidewall parts to prevent water loss

Step 7. Put the syrup basin + sidewalls in the freezer (-30˚) for a minimum of 24h to ensure that the syrup is frozen and (near-)solid (even if frozen at -30˚, it remains slightly fluid, Fig. 6).

Step 8. Put the frame with the viscous mixture representing the LLM in the freezer as well.

Step 9. Sieve in a thin <1 mm layer of Liaver or Zirshot beads to mark the base of the lithosphere in CT images (see section 4.5 for more info). Make sure to not sieve into the area between the inner sidewall and outer basin; if need be, cover these areas with the small lids (see Step 15)

Step 10. If sufficiently chilled, cut out the viscous layer representing the LLM from the frame (Fig. 12c), and put the layer on top of the frozen syrup. The easiest way to do so is to also cut the plastic sheet below (while keeping a bit of extra plastic on one short side to serve as a grip), and use that to move the layer into place (by first putting the short end without the plastic grip in place, against the short end of the model inset, and "unroll" the layer from the plastic sheet towards the opposite short end of the inset). If need be, since it is rather tricky, this can be done in two parts, and it might be good to dry-run the procedure a couple of times (Fig. 12c).

Step 11. As the LLM layer will not be 100% flat, let it flow out (the silicone-corundum sand mixture will flow at -30˚) for ca. 4 hours (with the lid on the basin), or until the surface of the LLM layer has become level

Step 12. Remove the basin from the freezer and install it on the Namazu (Fig. 14).

Step 13. Make sure that the motors have the correct starting coordinates for the given inner sidewall inset (overlapping plates or rubber, there may be a slight difference). Otherwise, the bars linking the inner sidewalls to the motors will not fit.

Step 14. Install the parts (plastic clamps) that keep the syrup basin in its correct place by fixing it to the base of the Namazu machine (Fig. 14).

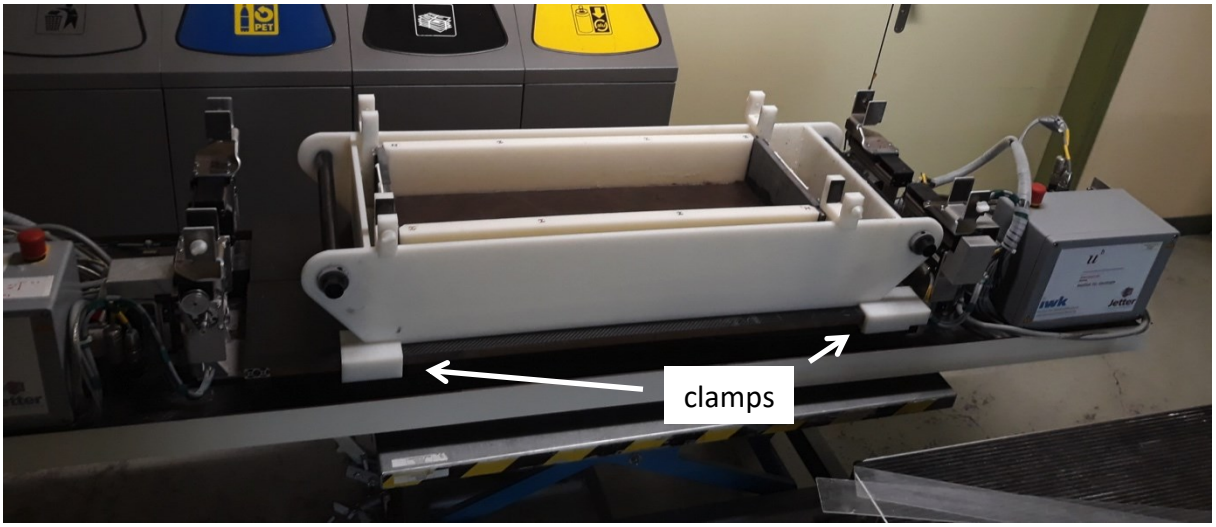

Figure 14. Installing the basin on the Namazu machine, and fixing it in the correct place using the clamps.

Step 15. Remove the lid that covers the whole machine, and install the smaller polystyrene lids that cover the syrup outside of the model domain (i.e. the areas between the inner sidewall and the syrup basin sidewalls, Fig. 15).

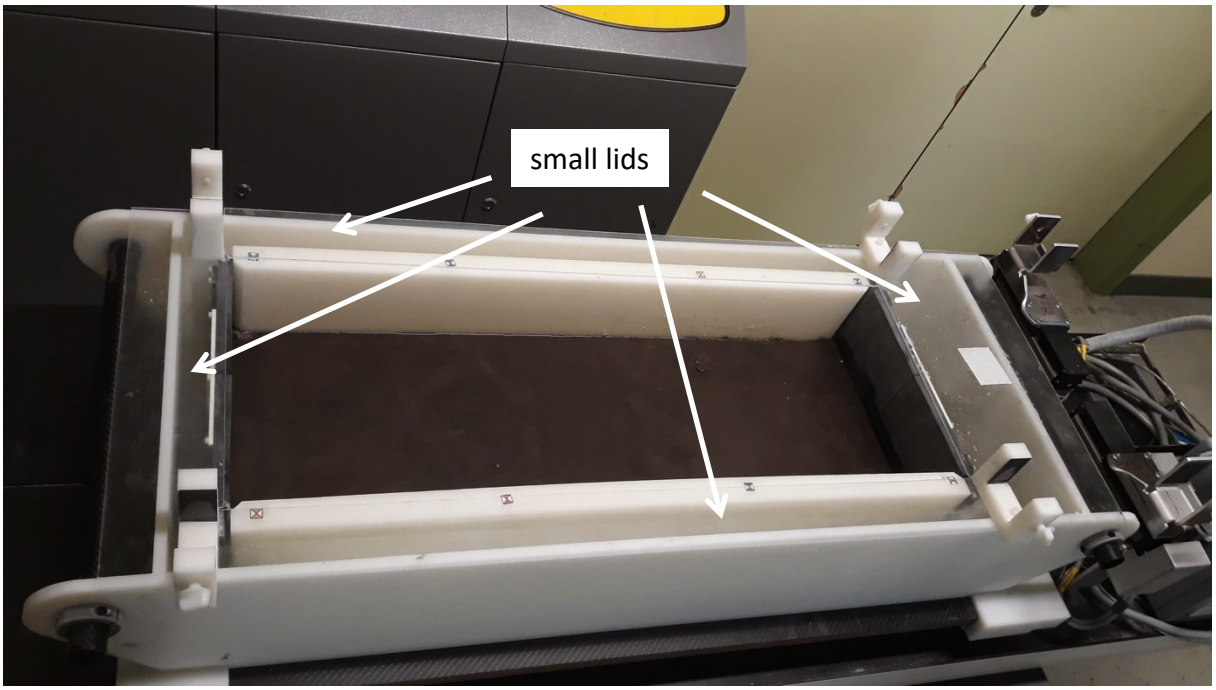

Figure 15. Using the small lids to cover the areas between the inner sidewall and the outer basin.

Step 16. Install a linear seed of viscous material representing a weakness in the ULM layer, if that is part of the model set-up (Fig. 16).

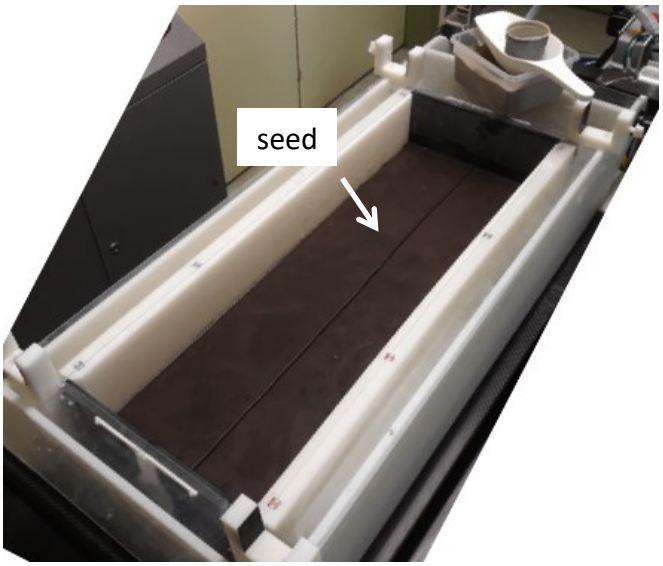

Figure 16. Applying a linear seed of viscous material that serves as an ULM weak zone in the model

Step 17. Sieve in the sand layer representing the ULM. Add layers of Zirshot or Liaver beads between brittle and viscous layers to generate layering on CT-imagery (see also section 4.5). Use a scraper to flatten the sand layers at the appropriate intervals, and regularly remove any condensation from the chilled model inner sidewalls (to avoid wetting the sand).

Step 18. Cut out the layer representing the LC from the frame (see Step 2) and add it carefully on top of the ULM layer.

Step 19. No time to wait for the LC layer to flow out (the syrup will thaw and the model will become unstable). Immediately sieve in the final sand layer representing the UC (Fig. 17a).

a) b)

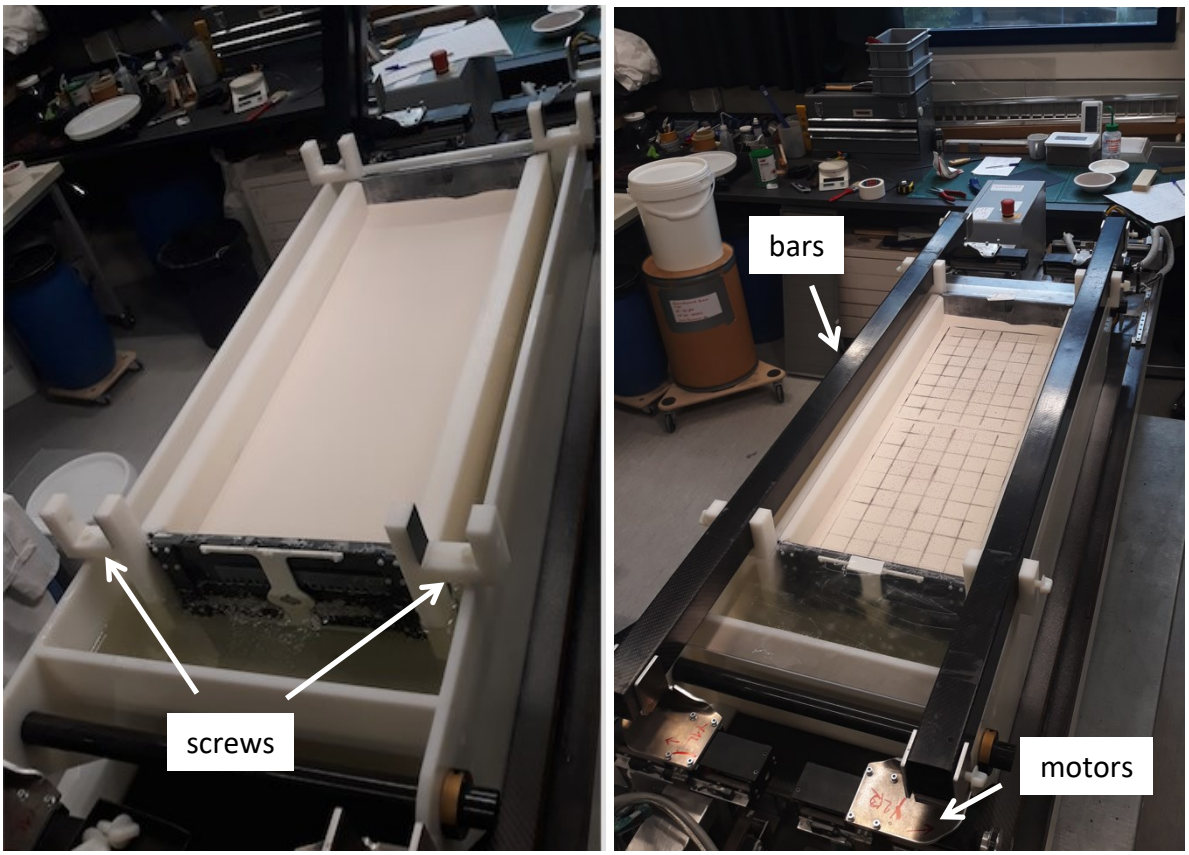

Figure 17. Adding model layers and preparing for the model run. (a) Added layers, contained by the inner model sidewalls. Note how the syrup level is lower than the top of the model layer. (b) Model prepared for a model run. For isostatic equilibrium, extra syrup is added so that it is at about the same level as the model layering (the exact level should be calculated though). The screws keeping the inner sidewalls are removed, and the bars that link the inner sidewalls to the motors are installed.

Step 20. Add the surface grid (corundum sand), and the coffee powder that serves as markers for DIC analysis (Figs. 4a, 17b).

Step 21. Clean away any left-over sand and remove the lids covering the syrup

Step 22. Add the appropriate amount of liquid syrup in the space between the inner sidewalls and the syrup basin sidewalls. Calculate the volume of the material needed to create isostatic equilibrium while maintaining the surface level of the model, the most practical method is to weigh the amount of syrup using a bathroom

scale. Make sure to take into account the syrup that sticks to the tools etc. A one-liter measuring cup is an excellent tool for scooping the syrup.

Step 23. Install (screw fixed) the parts on the motors that hold the bars (Fig. 17b).

Step 24. Carefully unscrew the four screws that keep the inner sidewalls in place (Figs. 11, 17a).

Step 25. Install the bars and screw them tight to fix them to the motors and inner sidewalls (Fig. 17b).

Step 26. Wait a night for the newly added syrup to flow out and fill the empty space, and for the frozen syrup to thaw.

Step 27. Move the modelling machine to the CT-scanner and lift it onto the CT-bed (Fig. 4b). Make sure it is in the right position to be properly covered by the camera rig that monitors surface deformation though time-lapse photography (check the height of the bed, and its initial position). To lift the machine onto the CT-bed, which is rather heavy, at least four people are required (at at every corner of the machine).

Step 28. Install the lighting (Fig. 4b).

Step 29. Install/link up and check the cameras (see section 4.3.1), adjust the camera position where necessary (Fig. 4b). Make sure the cameras are properly focussed on the model and connected to the central control computer, and check that the SD cards have sufficient space.

Step 30. Add a label with the model name and date on one of the bars (Fig. 18)

Step 31. Take pictures with the calibration plate for later DIC analysis (Fig. 19)

Step 32. Install the stopwatch and make sure its display is visible on all pictures (the lighting might reflect on the display, hiding the numbers)

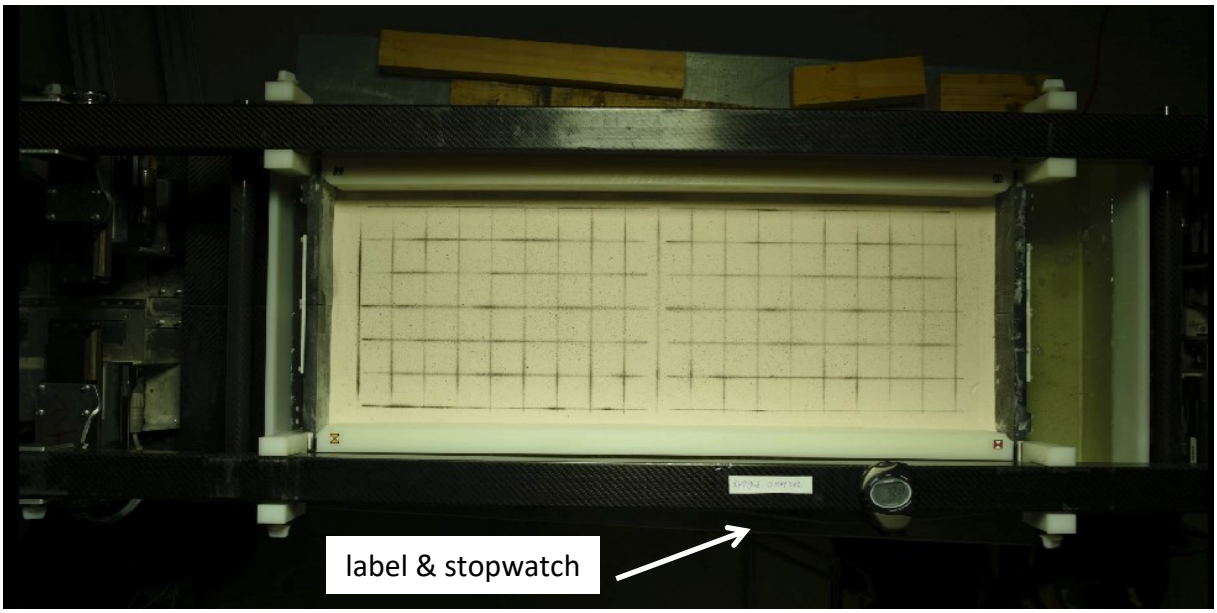

Figure 18. Top view picture before a model run. Note the model label and stopwatch.

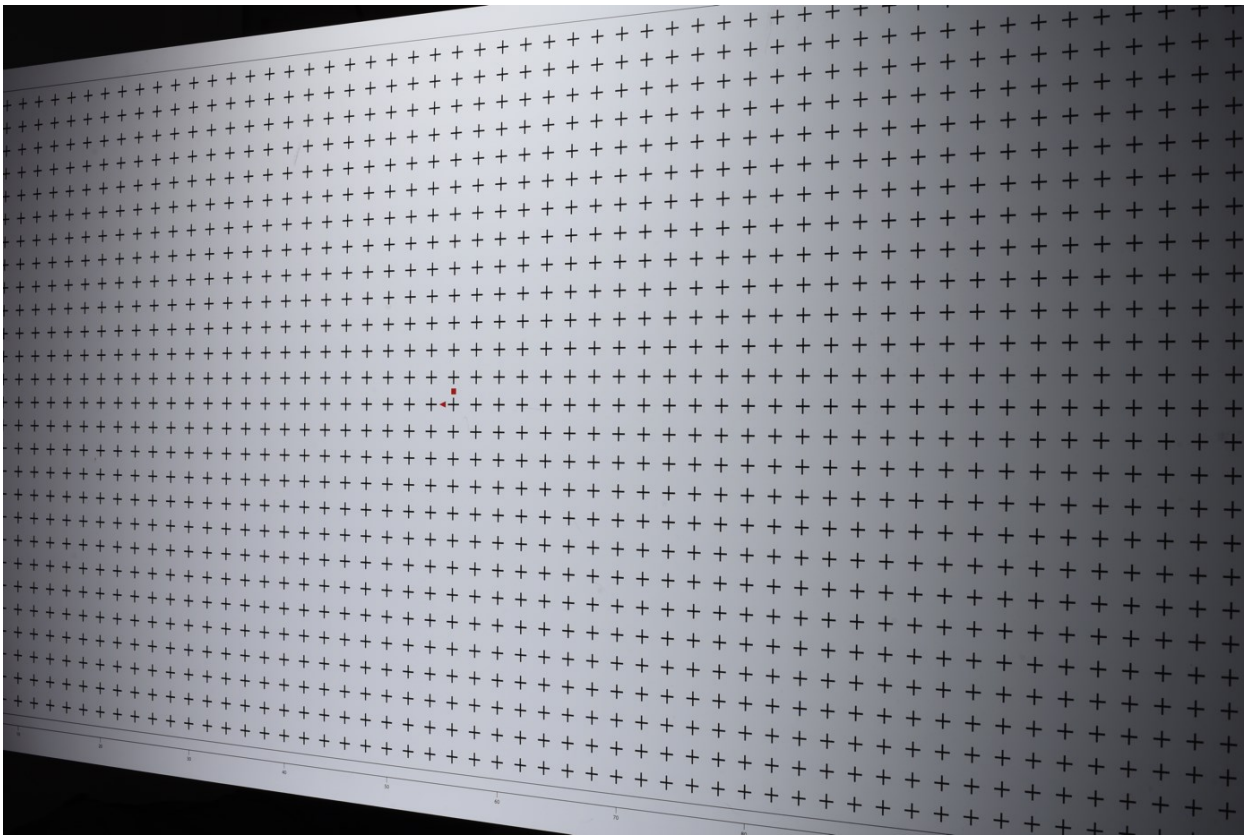

Figure 19. Inclined picture of the calibration plate, used to correct for distortion of the image for DIC analysis.

Step 33. Connect the Namazu machine to the control box and the computer. Carefully program the required deformation. Depending on the desired scanning interval and the rate of deformation, the machine can be halted during scanning or not. Too frequent scanning intervals mean that the scanner may need to cool down, so that it is better to halt the model while scanning (as is the case when applying high deformation rates, as scanning takes about a minute).

Step 34. Program the time-lapse photography protocol according to the scanning protocol (continued time-lapse over the whole model duration, or intermitted time-lapse between scanning intervals).

Step 35. Program the lighting (on/off) interval on the timer to fit the time-lapse protocol (half the interval duration of the time-lapse photography interval).

Step 36. Select how large the CT scan volume should be, double-check with the CT-technician if all settings are correct, and run the first CT scan.

Step 37. Run the model (start the machine, cameras and stopwatch) and collect data (time-lapse photography and CT-scanning, section 4.3, Fig. 4b). Regularly check if the machine is still running and if all cameras are still active.

Step 38. After completion of the model, recover the CT and time-lapse digital photographic data for analysis.

Step 39. Unscrew the bars connecting the inner sidewalls to the motors.

Step 40. Move the motors to the correct starting position

Step 41. Disconnect cameras, computers, modelling machine (cables etc.).

Step 42. Lift the machine from the CT bed and move it to the lab/preparation room (four people needed, see Step 27).

Step 43. Install the special lids to cover the syrup between the inner sidewalls and syrup basin walls.

Step 44. Carefully remove the UC, LC and ULM layers but leave the LLM in place.

Step 45. Remove the special lids

Step 46. Remove the syrup basin, containing the inner sidewalls and LLM layer, from the machine (after removing the clamps keeping it in place, Fig. 14), and put it in the freezer for a night too freeze (near-)solid.

Step 47. Take the syrup basin out of the freezer and remove the LLM (which remains viscous at -30˚, and is thus easily removable from the near-solid syrup. Use blunt knifes, spatulas, and similar tools.

Step 48. Leave the syrup basin out of the freezer for a day so that the syrup can thaw and find its level again. Do not try to clean the syrup any further once it is fluid again, that will only create a mess. Cover the syrup basin with the large lid if it will be exposed for longer periods of time.

Step 49. If a next model is planned, revert to step 1, otherwise, continue with the next step

Step 50. To clean the inner sidewall parts, fix the bars to the inner sidewalls only (i.e. the bars used to connect the inner sidewalls to the motors), carefully lift the inner sidewalls out of the syrup basin by handling the bars, and let them drip out into the syrup basin by having the bars rest at some elevated objects for some 30 minutes. Then fill a large basin (not the syrup basin) with lukewarm water and have the inner sidewalls hang into it for some 30 minutes, before removing the syrup rest. (Make sure to also cover the syrup basin with the appropriate lid to avoid exposure of the syrup and water loss). Best results are obtained when cleaning by hand (rubbing and scraping with finger[nail]s does the trick, allows easy detection of left-over syrup, and prevents damage to the plastic parts). After drying, all parts can be put in storage.

4.5. Challenges

4.5.1. Mechanical leeway

During our modelling runs for Zwaan & Schreurs (2023a), we noticed that some parts of the machine have a bit of mechanical leeway, so that deformation induced by the motors is not always fully transferred to the model lithosphere. This is due to the choice of material used for building the set-up: since plastics are not always fully rigid, especially in the case of plastic screws, such mechanical leeway may occur. However, after the initial stages of a model run, the limits of this leeway are reached, and deformation is fully transferred.

A possible solution could be the use of stiffer materials, even aluminium, which the Institute of Forensic Medicine (IRM) technicians in Bern have shown to be relatively X-ray transparent. However, the drawback of using stiffer materials could be that the set-up cannot accommodate the expansion and contraction of the syrup during model preparation, leading to cracks in the syrup basin. Such cracks would lead to leakage, fatally compromising the set-up. Hence, researchers may have to be careful when applying more rigid materials for lithospheric-scale model set-ups (if freezing is involved).

4.5.2. Visualization of model layering on CT-imagery - testing

We need some kind of markers to trace deformation in analogue models. In surface view, these markers can be coffee powder or some kind of grid (Figs. 17b, 18). Similar to natural systems, some sort of layering can be used to trace vertical deformation in models. When making traditional cross-sections, researchers can simply use differently coloured sand layers, which stand out against each other (e.g. Zwaan et al. 2020a, Fig. 20). However, such sectioning can only be done at the end of the model run, hence the need for CT-scanning, which allows the observation of internal model deformation over time. The challenge then becomes to create some sort of layering that is well visible on CT-imagery.

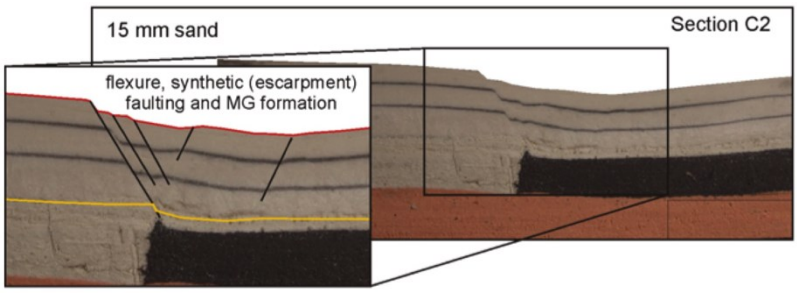

Figure 20. Cross-section showing final internal model structures from a model simulating marginal flexure. Insets show our structural interpretation. After Zwaan et al. (2020a). Model thickness: ca. 2.5 cm.

The primary factor controlling the visibility of materials on CT-scans (i.e. their intensity or colour on CT-imagery) is their relative attenuation values, which is largely a function of their density compared to the surrounding materials (e.g. Colletta et al. 2001). Simply put, materials with the same density tend to blend in on CT imagery (Fig. 21a), although internal textures may still be visible to a certain degree (e.g. granular materials with pores versus viscous materials without pores [or with air bubbles left over from mixing the original components], Fig. 21b). Hence, a straightforward method to generate layering on CT-imagery is to apply different layers with different densities, such as the alternating layering of quartz sand (ρ_{sieved} = 1560 kg/m3) and corundum sand (ρ_{sieved} = 1890 kg/m3) layering applied by Panien et al. (2005),

Zwaan et al. (2016) and Zwaan & Schreurs (2017) (Table 1, Fig. 22). However, a potential issue with this method is that the density profile of the materials is not 100% realistic. This does not seem to be much of an issue in the above-mentioned crustal-scale models, but the isostasy in lithospheric-scale models is highly sensitive to density variations. Therefore, a different method is desirable.

a) b)

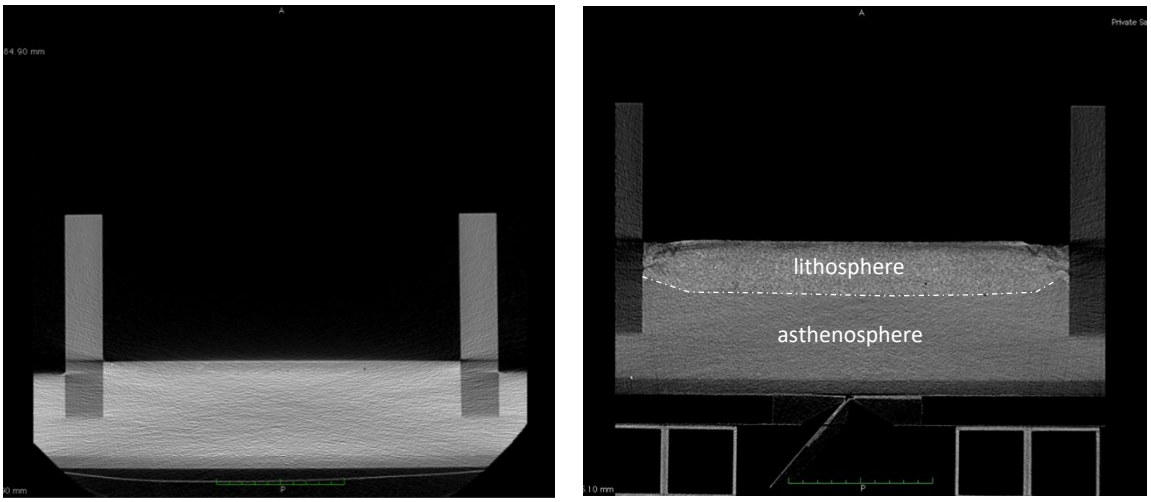

Figure 21. (In)visibility of material layering on CT-scans. (a) Scan of feldspar sand layer sieved on top of (frozen) syrup, where no distinction is visible between the feldspar sand and the underlying syrup. (b) Scan of Model A from Zwaan & Schreurs (2023a). Here the difference in texture between the (multilayer) model lithosphere allows it to be distinguished from the underlying syrup. But internal layering within the model lithosphere is not visible. Image widths: ca. 30 cm.

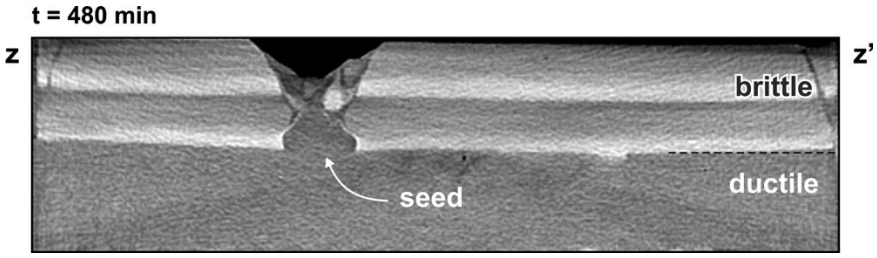

Figure 22. CT-section from a rifting model by Zwaan & Schreurs (2017), in which alternating corundum and quartz sand layers are applied to create clear layering in the brittle layer. The total model layering is 8 cm thick.

We opted to apply very thin layering of contrast materials instead, similar to the thin layering often used to trace deformation in traditional cross-sections (Fig. 20). We ran a series of tests to find out which material works best as a contrast material between (and within) layers. A first test (contrast test 1) involved five different granular materials: Zirshot beads (Z), quartz sand (Q), corundum sand (C), feldspar sand (F) and glass beads (G) (Fig. 23, Table 1). The quartz, corundum and feldspar sands are described in section 4.2, as well as in Zwaan & Schreurs (2023a), and references therein. The Zirshot beads are of ceramic origin (https://www.microbeads-ag.ch/), and have a high attenuation value (grain density),

compared to other making them stand out on CT-imagery. Glass beads are well-rounded beads that have a relatively low internal friction angle so that they can be used to simulate detachment layers or relatively weak basin infill (e.g. Panien et al. 2005, 2006). All materials we tested have similar densities when sieved (Table 1), even though the grain density (or specific gravity) of the Zirshot and corundum sand is rather high (ca. 4000 kg/m^3 vs. the <3000 kg/m^3 of the other materials). Still, the grain densities of all five materials are significantly higher than the density of the viscous mixture layer we applied in the test (1400 kg/m^3), and of the syrup as well (ca. 1450 kg/m^3).

Table 1. Properties of some granular materials used in Bern

Granular material	Grain size	Density (grain)	Density (bulk, sieved)
Zirshot beads (Z)[a]	150-210 µm	3850 kg/m^3	2300 kg/m^3
Quartz sand (Q)[b]	60-250 µm	2680 kg/m^3	1560 kg/m^3
Corundum sand (C)[c]	88-125 µm	4050 kg/m^3	1890 kg/m^3
Felspar sand (F)[d]	100-250 µm	2600-2700 kg/m^3	1300 kg/m^3
Glass beads (G)[b]	70-110 µm	2500 kg/m^3	1480 kg/m^3
Liaver beads[f]	100-300 µm	800 kg/m^3	530 kg/m^3

[a] Properties after Microbeads AG (product: „ceramic beads“), website: https://www.microbeads-ag.ch/

[b] Properties after Zwaan et al. (2018b) and Schmid et al. (2020)

[c] Properties after Panien et al. (2006)

[d] Properties after Willingshofer et al. (2019) and Zwaan et al. (2022b)

[e] Properties after Warsitzka et al. (2018)

We prepared a 1 cm thick viscous layer (See step 2 in section 4.4) and added a thin layer <1 mm of the materials in five separate domains. The idea was to have the materials stick to the viscous materials before applying the layer (rotating it, so that the granular materials end up between the syrup and sand), otherwise, the granular materials that do not stick to the viscous materials would simply sink into the syrup. On top of the viscous layer, we scooped in 2 cm of feldspar sand, and added some pre-cut faults in the sand, as well as some object (metal screws and pieces of wood) to test how well these are visualized as well.

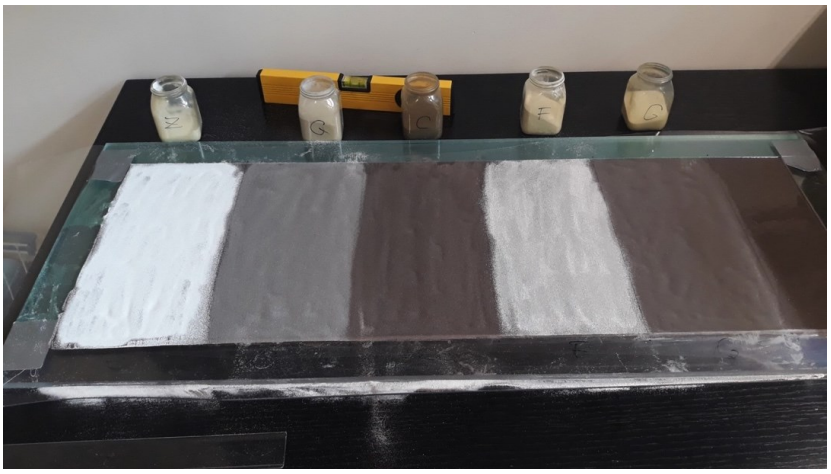

Figure 23. Layer surface and before putting it into the machine bottom side up for contrast test 1. From left to right: Zirshot (Z), quartz sand (Q), corundum sand (C), feldspar sand (F), and glass beads (G).

The results of this first contrast test are very clear: the only material of the five we tested creating a clear contrast on CT-imager are the Zirshot beads (Fig. 24). Also the pre-cuts in the sand layer are well visible, as these are planes along which the (overall) density of the material is strongly reduced. Comparing the cross-section in Figure 24b with the one in Figure 21a also highlights the impact of material handling on analogue models. In Figure 24b the feldspar sand was scooped in and the interface between it and the viscous layer below is well visible. By contrast, the feldspar sand/viscous layer interface is not visible in Figure 21a, which is highly likely due to the fact that the sand was sieved in (which is the standard procedure in Bern, to ensure constant material density within a model, and between models) (e.g. Klinkmüller et al. 2016; Zwaan et al. 2016; Schmid et al. 2020).

a)

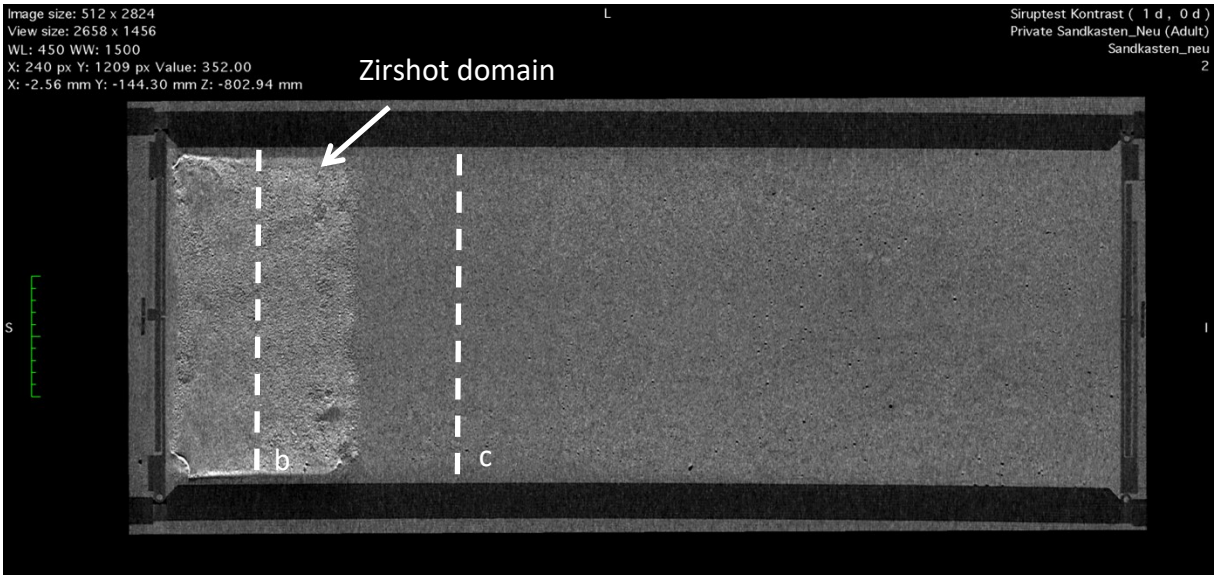

b)

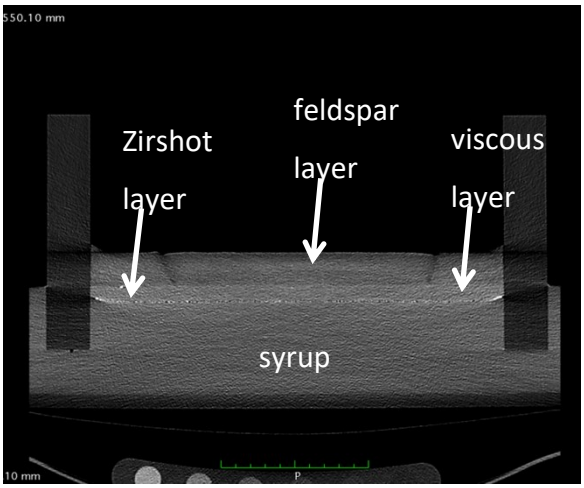

c)

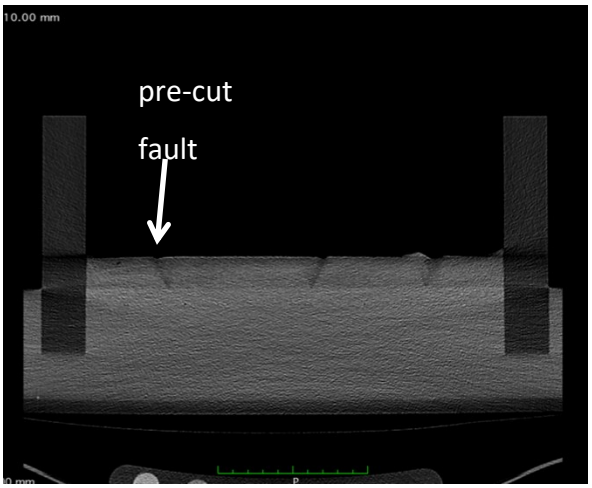

Figure 24. Results of first testing of contrast material for model layering (contrast test 1). (a) Horizontal cross-section trough the syrup-viscous layer interface, with only the Zirshot being visible (brighter grey to the left). (b) Cross-section through the area with the thin Zirshot layer highlighting the limit between the viscous layer and syrup below. (c) Cross-section through the area with the thin quartz sand layer (just next to the Zirshot area), which is invisible (compare to Fig. 21a). Note that in contrast to Fig. 21a, the feldspar-viscous mixture interface is visible. This is likely due to the handling method: in Fig. 21a, the feldspar sand was sieved in (which is the standard method in Bern, to ensure constant layer density within a model, and between models), whereas here, the feldspar sand was scooped in. Model width: ca. 30 cm.

A further observation we made in this test is the impact of high-density materials in a CT-scanner (Fig. 25). Low-density wood pieces appear in black. Zones of reduced sand density (pre-cuts in the sand) appear as darker lines. The metal screws, with their high density, are very bright instead, and cast "CT-shadows" to two sides, as they effectively block part of the X-rays from passing through. The orientation of these shadows indicated the orientation of the CT-scanning procedure (slices are taken perpendicular to the model axis).

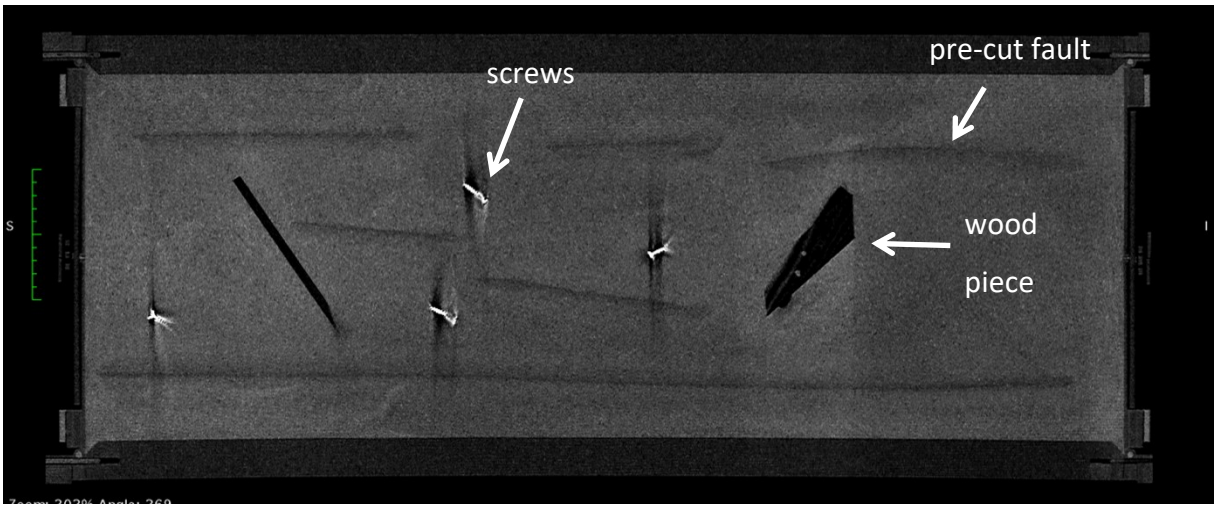

Figure 25. Horizontal CT section through the sand in contrast test 1, showing the pre-cut fault traces, the pieces of wood, and the metal screws which cast "CT-shadows". Model width: ca. 30 cm.

After determining the Zirshot beads as a viable contrast material on CT-scans, we also tested the application of low-density Liaver glass beads as a contrast material (contrast test 2, Fig. 26). These Liaver beads are hollow glass spheres with a sieved density of ca. 530 kg/m^3 (Warsitszka et al. 2019). We made a CT-scan of a small box (ca. 15 cm wide, Fig. 26) containing the following layering (bottom-to-top): syrup, thin Liaver layer, viscous mixture, thin Liaver layer, feldspar sand, thin Liaver layer, feldspar sand, thin Zirshot layer, feldspar sand. This test illustrates the basic viability of both Zirshot and Liaver beads as contrast materials in CT-scanned analogue models (Fig. 26).

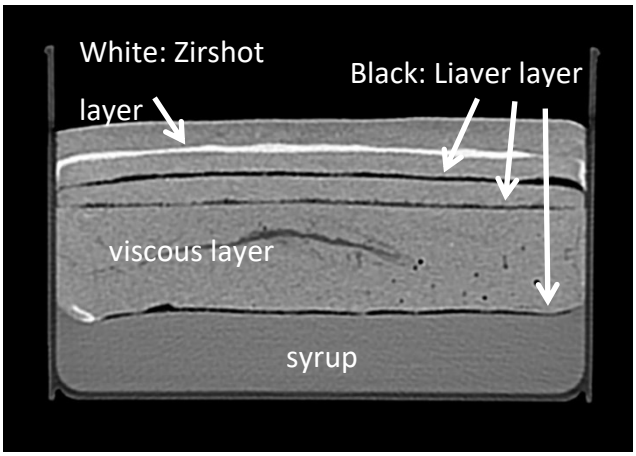

Figure 26. Contrast test 2. Vertical CT section showing how Zirshot and Liaver beads emphasize layering.

In our Zwaan & Schreurs (2023a) study we first opted for using the Liaver beads, and Model C (which was in fact the first CT-scanned model of that series) shows why (Fig. 27). In this model we applied Zirshot layering in the left-hand half of the model, and Liaver beads in the right-hand half. The Zirshot creates a very bright image (sections 1-3), whereas the Liaver layers provide a much more calm image, while still generating the desired layering on CT imagery (sections 4-6). As such, we decided to apply Liaver for future models, and focus on the part of the model with Liaver in our analysis of this particular model (Zwaan & Schreurs 2023a). Note that the choice of either Zirshot or Liaver beads does not impact the outcomes of the model analysis, but it improves the aesthetics and clarity of the imagery.

However, note the caveat when using such layering, highlighted by Model A from Zwaan & Schreurs (2023a) (Fig. 21b). In this model, with a reduced total model lithosphere thickness, the layering within the model lithosphere was not properly visible. Even so, the thickness of the internal layering (i.e. the distance between individual Liaver layers) was similar to that in Model C (Fig. 27), suggesting that the contrast layer thickness is the key factor: it should be ca. 1 mm thick to make sure these layers are visible on CT-scans.

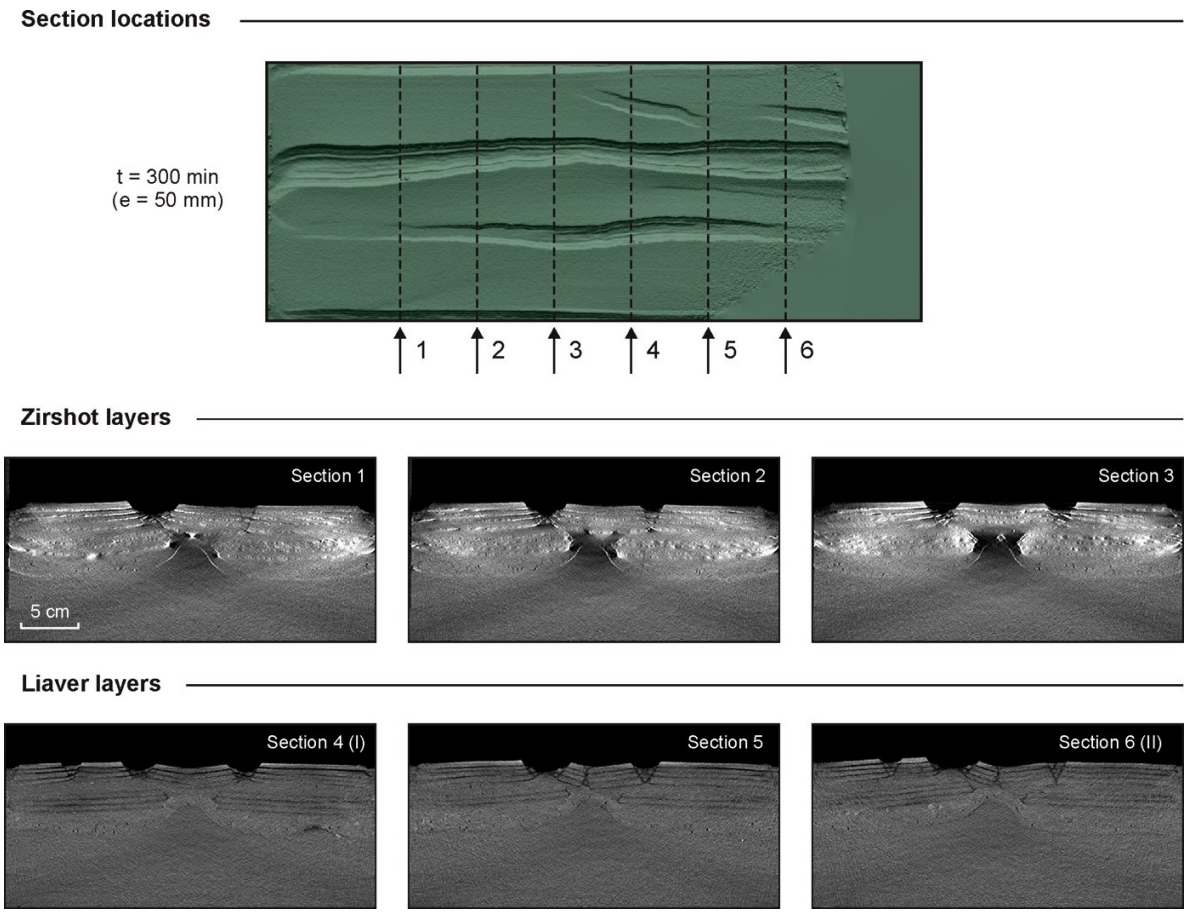

Figure 27. Comparison of Zirshot and Liaver bead layering in Model C from Zwaan & Schreurs (2023a). Top row: map-view of the model's final topography, and location of sections. Middle row: CT-sections from the model half with Zirshot layering at the end of the model run. Bottom row: CT-sections from the model half with Liaver layering at the end of the model run. Note that Sections 4 and 6 represent sections I and II in Zwaan & Schreurs (2023a), see also Figs. 7-9 for more details and annotation.

4.6. Potential for future modelling studies

The first models completed with this new procedure (Zwaan & Schreurs 2023a) prove the feasibility of running lithospheric-scale models of tectonic processes in a CT-scanner. From this point, many other such modelling efforts can be undertaken. For instance, different degrees of oblique extension (e.g. Mart & Dauteuil 2000; Autin et al. 2010, 2013), different lithospheric layering (e.g. no ULM brittle layer, see e.g. Allemand et al. 1989; Brun 2002), or the emplacement of linear viscous seeds in the UC or with different orientations, see Molnar et al. 2019; 2020). If need be a plastic sheet can be put at the base of the LC layer (Sun et al. 2009). And other than rifting models, compressional tectonics can be simulated as well (e.g. Willingshofer & Sokoutis 2009; Luth et al. 2010; Sokoutis & Willingshofer 2011; Willingshofer et al. 2013; Calignano et al. 2015; 2017). A further step will be the application of digital volume correlation (DVC) on CT-data. This method, which applies DIC techniques to a volume, rather than a surface, has been used to analyse model-internal deformation in brittle-only and brittle-viscous crustal-scale models (e.g. Adam et al. 2013; Zwaan et al. 2018a; Schmid et al. 2022a, 2022b), but so far not on lithospheric-scale models (for the obvious reason that no CT-data were available so far).

5. Acknowledgements

The basic inspiration for this new machine was sparked by discussions with Yago Nestola, who was working at the University of Parma at the time. We would furthermore like to thank the engineers from IPEK Rapperswil (Dario Niggli, Peter Eichenberger, Theodor Wüst) for working out our initial design and for constructing the components for the new model set-up. We are grateful to Prof. Christian Jackowski for granting access to the CT-scanner of the Institute of Forensic Medicine (IRM) in Bern and to Nicole Schwendener for help in CT-data acquisition. Discussions with Nicolas Molnar helped to improve the model design. Thanks also to Timothy Schmid from our Tectonic Modelling group for helping with the DIC analysis, and to Kirsten Elger and Florian Ott from GFZ Potsdam for helping us in preparing this GFZ data publication. This research was funded by the Swiss National Science Foundation, grant 200021-178731 "4D Analogue modelling of oblique rifts and obliquely rifted margins" (https://data.snf.ch/grants/grant/178731).

6. References

Adam, J., Klinkmüller, M., Schreurs, G., & Wieneke, N. (2013). Quantitative 3D strain analysis in analogue experiments simulating tectonic deformation: Integration of X-ray computed tomography and digital volume correlation techniques. Journal of Structural Geology, 55, 127-149. http://doi.org/10.1016/j.jsg.2013.07.011

Allemand, P., & Brun, J. -P. (1991). Width of continental rifts and rheological layering of the lithosphere. Tectonophysics, 188, 63-69. https://doi.org/10.1016/0040-1951(91)90314-I

Allemand, P., Brun, J. -P., Davy, P., & Van den Driessche, J. (1989). Symétrie et asymétrie des rifts et mécanismes d'amincissement de la lithosphere. Bulletin de la Société Géologique de France, V(3), 423-436. https://doi.org/10.2113/gssgfbull.V.3.423

Alonso-Henar, J., Schreurs, G., Martinez-Díaz, J. J., Álvarez-Gómez, J. A., & Villamor, P. (2015). Neotectonic development of the El Salvador Fault Zone and implications for deformation in the Central America Volcanic Arc: Insights from 4-D analog modeling experiments. Tectonics, 34, 133–151. https://doi.org/10.1002/2014TC003723

Autin, J., Bellahsen, N., Husson, L, Beslier, M.-O., Leroy, S., & d'Acremont, E. (2010). Analog models of oblique rifting in a cold lithosphere, Tectonics, 29, TC6016. https://doi.org/10.1029/2010TC002671

Autin, J., Bellahsen, N., Leroy, S., Husson, L., Beslier, M.-O.-M., & d'Acremong, E., (2013). The role of structural inheritance in oblique rifting: Insights from analogue models and application to the Gulf of Aden. Tectonophysics, 607, 51-64. https://doi.org/10.1016/j.tecto.2013.05.041

Benes, V., & Davy, P. (1996). Modes of continental lithospheric extension: experimental verification of strain localization processes. Tectonophysics, 254, 69-87. https://doi.org/10.1016/0040-1951(95)00076-3

Benes, V., & Scott, S.D. (1996). Oblique rifting in the Havre Trough and its propagation into the continental margin of New Zealand: comparison with analogue experiments. Marine Geophysical Researches, 18, 189-201. https://doi.org/10.1007/BF00286077

Beniest, A., Willingshofer, E., Sokoutis, D., & Sassi, W. (2018). Extending continental lithosphere with lateral strength variations: effects on deformation localization and margin geometries. Frontiers in Earth Science, 6, 148. https://doi.org/10.3389/feart.2018.00148

Beslier, M. -O. (1991). Formation des marges passives et remontée du manteau : Modélisation expérimentale et exemple de la marge de la Galice. Memoires et documents du Centre Armoricain

d'etude structurale des socle, (Doctoral Dissertation). Retrieved from HAL (https://tel.archives-ouvertes.fr/tel-00594598). University Rennes 1, France.

Boutelier, D., Schrank, C., & Regenauer-Lieb, K. (2019). 2-D finite displacements and strain from particle imaging velocimetry (PIV) analysis of tectonic analogue models with TecPIV. Solid Earth, 10, 1123-1139. https://doi.org/10.5194/se-10-1123-2019

Brun, J. -P. (2002). Deformation of the continental lithosphere: Insights from brittle-ductile models. Geological Society, London, Special Publications, 200, 355-370. https://doi.org/10.1144/GSL.SP.2001.200.01.20

Brun, J. -P., & Beslier, M.-O. (1996). Mantle exhumation at passive margins. Earth and Planetary Science Letters 142, 161-173. https://doi.org/10.1016/0012-821X(96)00080-5

Calignano, E., Sokoutis, D., Willingshofer, E., Gueydan, F., & Cloetingh, S. (2015). Asymmetric vs. symmetric deep lithospheric architecture of intra-plate continental orogens. Earth and Planetary Science Letters, 424, 38-50. https://doi.org/10.1016/j.epsl.2015.05.022

Calignano, E., Sokoutis, Willingshofer, E., Brun, J.-P., Gueydan, F., & Cloetingh, S. (2017). Oblique contractional reactivation of inherited heterogeneities: Cause for arcuate orogens. Tectonics, 36, 542-558. https://doi.org/10.1002/2016TC004424

Capelletti, A., Tsikalas, F., Nestola, Y., Cavozzi, C., Argnani, A., Meda, M., & Salvi, F. (2013). Impact of lithospheric heterogeneities on continental rifting evolution: Constraints from analogue modelling on South Atlantic margins. Tectonophysics, 608, 30-50. https://doi.org/10.1016/j.tecto.2013.09.026

Colletta, B., Letouzey, J., Pinedo, R., Ballard, J. F., & Balé, P. (1991). Computerized X-ray tomography analysis of sandbox models: Examples of thin-skinned thrust systems. Geology, 19(11), 1063-1067. https://doi.org/10.1130/0091-7613(1991)019<1063:CXRTAO>2.3.CO;2

Fedorik, J., Zwaan, F., Schreurs, G., Toscani, G., & Bonini, L. (2019). The interaction between strike-slip dominated fault zones and thrust belt structures: Insights from 4D analogue models. Journal of Structural Geology, 122, 89-105. https://doi.org/10.1016/j.jsg.2019.02.010

Klinkmüller, M. (2011). Properties of analogue materials, experimental reproducibility and 2D/3D deformation quantification techniques in analogue modeling of crustal-scale processes, (Doctoral dissertation). Location: University of Bern, Switzerland.

Klinkmüller, M., Schreurs, G., Rosenau, M., Kemnitz, H. (2016). Properties of granular analogue model materials: A community wide survey. Tectonophysics, 684, 23–38. http://doi.org/10.1016/j.tecto.2016.01.017

Letouzey, J., Colletta, B., Vially, R., & Chermette, J. C. (1995). Evolution of Salt-Related Structures in Compressional Settings. In: Jackson, M. P. A., Roberts, D. G., & Snelson, S. (Eds.). Salt tectonics: a global perspective. AAPG Memoir, 65, 41-60. https://doi.org/10.1306/M65604C3

Luth, S., Willingshofer, E., Sokoutis, D., & Cloetingh, S. (2010). Analogue modelling of continental collision: Influence of plate coupling on mantle lithosphere subduction, crustal deformation and surface topography. Tectonophysics, 484, 87-102. https://doi.org/10.1016/j.tecto.2009.08.043

Mart, Y., & Dauteuil, O. (2000). Analogue experiments of propagation of oblique rifts. Tectonophysics 3016, 121-132. https://doi.org/10.1016/S0040-1951(99)00231-0

Molnar, N. E., Cruden, A. R., & P. G. Betts (2017). Interactions between propagating rotational rifts and linear rheological heterogeneities: Insights from three-dimensional laboratory experiments. Tectonics, 36, 420–443. https://doi.org/10.1002/2016TC004447

Molnar, N. E., Cruden, A. R., & P. G. Betts (2018). Unzipping continents and the birth of microcontinents. Geology, 46(5), 451-454. https://doi.org/10.1130/G40021.1

Molnar, N. E., Cruden, A.R., & Betts, P.G. (2019). Interactions between propagating rifts and linear weaknesses in the lower crust. Geosphere, 15. https://doi.org/10.1130/GES02119.1

Molnar, N. E., Cruden, A.R., & Betts, P.G. (2020). The role of inherited crustal and lithospheric architecture during the evolution of the Red Sea: Insights from three dimensional analogue experiments. Earth and Planetary Science Letters, 54, 116377. https://doi.org/10.1016/j.epsl.2020.116377

Nestola, Y., Storti, F., & Cavozzi, C. (2015). Strain rate-dependent lithosphere rifting and necking architectures in analog experiments. Journal of Geophysical Research: Solid Earth, 120, 584-594. https://doi.org/10.1002/2014JB011623

Nestola, Y., Storti, F., Bedogni, E., & Cavozzi, C. (2013). Shape evolution and finite deformation pattern in analog experiments of lithosphere necking. Geophysical Research Letters, 40, 5025-5057. https://doi.org/10.1002/grl.50978

Panien, M., Schreurs, G., & Pfiffner, A. (2005). Mechanical behaviour of granular materials used in analogue modelling: insights from grain characterisation, ring-shear tests and analogue experiments. Journal of Structural Geology, 28, 1710-1724. https://doi.org/10.1016/j.jsg.2006.05.004

Panien, M., Schreurs, G., & Pfiffner, A. (2005). Sandbox experiments on basin inversion: testing the influence of basin orientation and basin fill. Journal of Structural Geology, 27, 433-445. https://doi.org/10.1016/j.jsg.2004.11.001

Richard, P. (1989). Champs de failles au dessus d'un déchrochement de socle: modélisation expérimentale. Memoires et documents du Centre Armoricain d'etude structurale des socle, (Doctoral Dissertation). Retrieved from HAL (https://tel.archives-ouvertes.fr/tel-00675425/document). University Rennes 1, France.

Samsu, A., Cruden, A. R., Molnar, N. E., & Weinberg, R. F. (2021). Inheritance of penetrative basement anisotropies by extension-oblique faults: Insights from analogue experiments. *Tectonics*, *40*, e2020TC006596. https://doi.org/10.1029/2020TC006596

Sassi, W., Colletta, B., Balé, P., & Paquereau, T. (1993). Modelling of structural complexity in sedimentary basins: the role of pre-existing faults in thrust tectonics. Tectonophysics, 226, 97-112. https://doi.org/10.1016/0040-1951(93)90113-X

Schmid, T. C., Schreurs, G., Adam, J. (2022a). Characteristics of continental rifting in rotational systems: New findings from spatiotemporal high resolution quantified crustal scale analogue models. Tectonophysics, 822, 229174. https://doi.org/10.1016/j.tecto.2021.229174

Schmid, T. C., Schreurs, G., Adam, J. (2022b). Rotational Extension Promotes Coeval Upper Crustal Brittle Faulting and Deep-Seated Rift-Axis Parallel Flow: Dynamic Coupling Processes Inferred From Analog Model Experiments. Journal of Geophysical Research: Solid Earth, 127, e2022JB024434. https://doi.org/10.1029/2022JB024434

Schmid, T., Schreurs, G., Warsitzka, M., Rosenau, M. (2020). Effect of sieving height on density and friction of brittle analogue material: Ring-shear test data of quarz sand used for analogue experiments in the Tectonic Modelling Lab of the University of Bern. GFZ Data Services. https://doi.org/10.5880/fidgeo.2020.006

Schmid, T., Zwaan, F., Corbi, F., Funiciello, F., & Schreurs, G. (2022c). Rheology of glucose syrup from the Tectonic Modelling Lab (TecLab) of the University of Bern (CH). GFZ Data Publication. https://doi.org/10.5880/fidgeo.2022.030

Schori, M., Zwaan, F., Schreurs, G., Mosar, J. (2021). Pre-existing Basement Faults Controlling Deformation in the Jura Mountains Fold-and-Thrust Belt: Insights from Analogue Models. Tectonophysics, 814, 228980. https://doi.org/10.1016/j.tecto.2021.228980

Schreurs, G., & Colletta, B. (1998). Analogue modelling of continental transpression. In: Schellart , W. P. and Passchier, C. (Eds). Analogue modelling of large-scale tectonic processes. Journal of the Virtual Explorer , 7, 103-114. http://doi.org/10.3809/jvirtex.2002.00040

Schreurs, G., & Colletta, B. (1998). Analogue modelling of faulting in zones of continental transpression and transtension. Geological Society, London, Special Publications 1998, 135, 59-79. https://doi.org/10.1144/GSL.SP.1998.135.01.05

Schreurs, G., Buiter, S. J. H., Boutelier, J., Burberry, C., Callot, J. -P., Cavozzi, C., Cerca, M., Chen, J.- H. H., Cristallini, E., Cruden, A. R., Cruz, L., Daniel, J.-M., Da Poian, G., Garcia, V. H., Gomes, C.J.S., Grall, C., Guillot, Y., Guzmán, C., Hidayah, T. N., Hilley, G. E., Klinkmüller, M., Koyi, H. A., Lu, C. -Y. Y., Maillot, B., Meriaux, C., Nilfouroushan, F., Pan, C. -C. C., Pillot, D., Portillo, R., Rosenau, M., Schellart, W.P., Schlische, R. W., Take, A., Vendeville, B. C., Vergnaud, M., Vettori, M., Wang, S. -H. H., Withjack, M.O., Yagupsky, D., & Yamada, Y. (2016). Benchmarking analogue models of brittle thrust wedges, Journal of Structural Geology, 92, 116–139. https://doi.org/10.1016/j.jsg.2016.03.005.

Schreurs, G., Buiter, S.J.H., Boutelier, D., Corti, G., Costa, E., Cruden, A.R., Daniel, J.-M., Hoth, S., Koyi, H.A., Kukowski, N., Lohrmann, J., Ravaglia, A., Schlische, R.W., Withjack, M.O., Yamada, Y., Cavozzi, C., Del Ventisette, C., Brady, J.A.E., Hoffmann-Rothe, A., Mengus, J.-M., Montanari, D., Nilforoushan, F., 2006. Analogue benchmarks of shortening and extension experiments. SP 253, 1–27. https://doi.org/10.1144/GSL.SP.2006.253.01.01

Schreurs, G., Hänni, R., & Vock, P. (2002a). The influence of brittle-viscous multilayers on faulting during rifting: an analogue modelling approach. In: Schellart, W. P. and Passchier, C. W. (Eds). Analogue modelling of large-scale tectonic processes. Journal of the Virtual Explorer, 7, 89-96. http://doi.org/10.3809/jvirtex.2002.00042

Schreurs, G., Hänni, R., & Vock, P. (2002b). Analogue modelling of transfer zones in fold and thrust belts: a 4-D analysis. In: Schellart , W. P. and Passchier, C. (Eds). Analogue modelling of large-scale tectonic processes. Journal of the Virtual Explorer, 7, 67-73. http://doi.org/10.3809/jvirtex.2002.00047

Schreurs, G., Hänni, R., & Vock, P. (2003). Analysis of analogue models by helical X-ray computed tomography. In: Mees, F., Swennen, R., Van Geet, M., Jacobs, P. (Eds.) Applications of X-ray Computed Tomography in the Geosciences. Geological Society, London, Special Publications, 215, 213-223. https://doi.org/10.1144/GSL.SP.2003.215.01.20

Sokoutis, D., & Willingshofer, E. (2011). Decoupling during continental collision and intra-plate deformation. Earth and Planetary Science Letters, 305, 435–444. https://doi.org/10.1016/j.epsl.2011.03.028

Sun, Z., Zhong, Z., Keep, M., Zhou, D., Cai, D., Li, X., Wu, S., & Jiang, J. (2009). 3D analogue modeling of the South China Sea: A discussion on breakup pattern. Journal of Asian Earth Sciences, 34, 544–556. https://doi.org/10.1016/j.jseaes.2008.09.002

Warsitzka, M., Ge, A., Schönebeck, J.-M., Pohlenz, A., & Kukowski, N. (2019). Ring-shear test data of foam glass beads used for analogue experiments in the Helmholtz Laboratory for Tectonic Modelling (HelTec) at the GFZ German Research Centre for Geosciences in Potsdam and the Institute of Geosciences, Friedrich Schiller University Jena. GFZ Data Services. https://doi.org/10.5880/GFZ.4.1.2019.002

Willingshofer, E., & Sokoutis, D. (2009). Decoupling along plate boundaries: Key variable controlling the mode of deformation and the geometry of collisional mountain belts. Geology, 37(1), 39-42. https://doi.org/10.1130/G25321A.1

Willingshofer, E., Sokoutis, D., Beekman, F., Schönebeck, J.-M., Warsitzka, M., & Rosenau, M. (2018). Ring shear test data of feldspar sand and quartz sand used in the Tectonic Laboratory (TecLab) at Utrecht University for experimental Earth Science applications. V. 1. GFZ Data Services. https://doi.org/10.5880/fidgeo.2018.072

Willingshofer, E., Sokoutis, D., Luth, S. W., Beekman, F., & Cloetingh, S. (2013). Subduction and deformation of the continental lithosphere in response to plate and crust-mantle coupling. Geology, 41(12), 1239-1242. https://doi.org/10.1130/G34815.1

Zwaan, F. (2017). 4D laboratory experiments of oblique extension and scissor tectonics, structural inheritance and sedimentation: implications for rift evolution, rift propagation and rift segment interaction (Doctoral Dissertation). Retrieved from BORIS (https://boristheses.unibe.ch/824/) University of Bern, Switzerland.

Zwaan, F., & Schreurs, G. (2015). Effects of transtension on continental rift interaction: a 4D analogue modeling study. Geotectonic Research, 97, 116-119. https://doi.org/10.1127/1864-5658/2015-44

Zwaan, F., & Schreurs, G. (2017). How oblique extension and structural inheritance influence rift segment interaction: Insights from 4D analog models. Interpretation, 5, SD119-SD138. http://doi.org/10.1190/INT-2016-0063.1

Zwaan, F., & Schreurs, G. (2023). Analogue models of lithospheric-scale rifting monitored in an X-ray CT scanner. Tectonics, 41, e2022TC007291. https://doi.org/10.1029/2022TC007291

Zwaan, F., & Schreurs, G. (2023b). Digital image correlation (DIC) and X-Ray CT analyses of lithospheric-scale analogue models of continental rifting. GFZ Data Services. https://doi.org/10.5880/fidgeo.2023.006

Zwaan, F., Chenin, P., Erratt, D., Manatschal, G., & Schreurs, G. (2021a). Complex rift patterns, a result of interacting crustal and mantle weaknesses, or multiphase rifting? Insights from analogue models. Solid Earth, 12, 1473-1495. https://doi.org/10.5194/se-12-1473-2021

Zwaan, F., Chenin, P., Erratt, D., Manatschal, G., & Schreurs, G. (2022a). Competition between 3D structural inheritance and kinematics during rifting: Insights from analogue models. Basin Research, 00, 1-31. https://doi.org/10.1111/bre.12642

Zwaan, F., Corti, G., Keir, D., Sani, F. (2020a). Analogue modelling of marginal flexure in Afar, East Africa: Implications for passive margin formation. Tectonophysics, 796, 228595. https://doi.org/10.1016/j.tecto.2020.228595

Zwaan, F., Scheurs, G., Rudolf, M., & Rosenau, M. (2022b). Ring-shear test data of feldspar sand FS 900 S used in the Tectonic Modelling Laboratory at the University of Bern (Switzerland). GFZ Data Services. https://doi.org/10.5880/fidgeo.2022.008

Zwaan, F., Schreurs, G., & Adam, J. (2018a). Effects of sedimentation on rift segment evolution and rift interaction in orthogonal and oblique extensional settings: Insights from analogue models analysed with 4D X-ray computed tomography and digital volume correlation techniques. Global and Planetary Change, 171, 110-133. https://doi.org/10.1016/j.gloplacha.2017.11.002

Zwaan, F., Schreurs, G., & Buiter, S. J. H. (2019). A systematic comparison of experimental set-ups for modelling extensional tectonics. Solid Earth, 1010, 1063-1097. https://doi.org/10.5194/se-10-1063-2019

Zwaan, F., Schreurs, G., & Rosenau, M. (2020b). Rift propagation in rotational versus orthogonal extension: Insights from 4D analogue models. Journal of Structural Geology, 135, 103946. https://doi.org/10.1016/j.jsg.2019.103946

Zwaan, F., Schreurs, G., Gentzmann, R., Warsitzka, M., & Rosenau, M. (2018b). Ring-shear test data of quartz sand from the Tectonic Modelling Lab of the University of Bern (CH). V. 1. GFZ data Services. https://doi.org/10.5880/fidgeo.2018.028

Zwaan, F., Schreurs, G., Naliboff, J., & Buiter, S. J. H. (2016). Insights into the effects of oblique extension on continental rift interaction from 3D analogue and numerical models. Tectonophysics, 693, 239-260. http://doi.org/10.1016/j.tecto.2016.02.036

Zwaan, F., Schreurs, G., Ritter, M., Santimano, T., & Rosenau, M. (2018c). Rheology of PDMS-corundum sand mixtures from the Tectonic Modelling Lab of the University of Bern (CH). V. 1. GFZ data Services. https://doi.org/10.5880/fidgeo.2018.023